The Meteoritical Society

Meteoritics & Planetary Science 57, Nr 12, 2192–2215 (2022)
doi: 10.1111/maps.13925

Shidian meteorite, a new fall analog of near-Earth asteroid (101955) Bennu

Yan FAN[1,2], Shijie LI[2,3]*, Shen LIU[1]*, Qingzhu YIN[4], Guangming SONG[5], Rui XU[6], Jiang ZHANG[7], Pengfei ZHANG[8], Chengyu LIU[6], Rong WANG[6], and Thomas SMITH[9]

[1]State Key Laboratory of Continental Dynamics and Department of Geology, Northwest University, Xi'an 710069, China
[2]Center for Lunar and Planetary Sciences, Institute of Geochemistry, Chinese Academy of Sciences, Guiyang 550081, China
[3]Chinese Academy of Sciences Center for Excellence in Comparative Planetology, Hefei 230026, China
[4]Department of Earth & Planetary Sciences, University of California at Davis, One Shields Avenue, Davis, California 95616, USA
[5]Beijing Institute of Spacecraft Environment Engineering, Beijing 100094, China
[6]Key Laboratory of Space Active Opto-Electronics Technology, Shanghai Institute of Technical Physics, Chinese Academy of Sciences, Shanghai 200083, China
[7]Shandong Key Laboratory of Optical Astronomy and Solar-Terrestrial Environment, School of Space Science and Physics, Institute of Space Sciences, Shandong University, Weihai 264209, China
[8]State Key Laboratory of Lunar and Planetary Sciences, Macau University of Science and Technology, Macau 999078, China
[9]State Key Laboratory of Lithospheric Evolution, Institute of Geology and Geophysics, Chinese Academy of Sciences, Beijing 100029, China
*Corresponding author. E-mail: lishijielpsc@mail.gyig.ac.cn (S. Li); liushen@nwu.edu.cn (S. Liu)

(Received 12 July 2022; revision accepted 17 October 2022)

Abstract–Shidian is a recent meteorite which fell in Yunnan province, China, on November 27, 2017, and has been classified as a CM2 chondrite. Petrography, mineralogy, oxygen and chromium isotopic composition, reflectance spectrum, and density studies of Shidian are reported in this study. Clasts with different aqueous alteration degree, two type 1 clasts with nontypical CM petrography, and one metamorphic clast are observed in Shidian. Mineralogically, Shidian main body consists of phyllosilicates (~70 vol%), forsterite (~13 vol%), fayalitic olivine, carbonates, sulfide, high-Ca pyroxene, magnetite framboids, and Fe-Ni metal. The average electron microprobe analysis (EMPA) analytical totals of phyllosilicates are 84.07 ± 1.75 wt%, with average FeO/SiO_2 of tochilinite–cronstedtite intergrowths (TCIs) in different clasts ranging from 1.18 to 3.29. The bulk geochemical composition is characterized by flat rare earth element pattern, and by depletion of highly volatile elements. The whole rock oxygen isotopic composition is −0.51 ± 0.73‰, 5.44 ± 1.01‰, and −3.38 ± 0.20‰ for $\delta^{17}O$, $\delta^{18}O$, and $\Delta^{17}O$, respectively, with bulk chromium isotopic composition as $\varepsilon^{54}Cr = 1.00 \pm 0.11$. The grain density, bulk density, and porosity are 2.758 ± 0.008 g cm^{-3}, 2.500 ± 0.004 g cm^{-3}, and 9.37 ± 0.59%, respectively. The reflectance spectrum shows "blue" (negative) continuum slope across the visible and near-infrared range, with characteristic absorption features (such as 0.765, 0.923, and 1.160 μm for phyllosilicates). These characteristics indicate that Shidian is an unheated, brecciated CM chondrite and may be an analog of asteroid Bennu.

INTRODUCTION

Carbonaceous chondrites (CC) are primitive extraterrestrial rocks formed over 4.5 billion years ago in the solar nebula, are rare types of meteorites, and account for about 4.4% of chondritic meteorite falls and finds (Ray & Shukla, 2018; Rudraswami et al., 2019). In addition, CC are characterized by high content of bound (structural) water, which can reach up to ~20 wt% (such as Orgueil, Ivuna, and Tonk) and are distinguishable from ordinary chondrites (~0.1 wt%, up to 2 wt%) and enstatite chondrites (ECs, ~0.1 wt%) (Dodd et al., 1967; Hutchison, 2004; Krot et al., 2003; Weisberg et al., 2006; Wiik, 1956; Wu et al., 2018), although the water contents

of some groups (e.g., CO, CK, CH, CB) are less than 1% (Velbel et al., 2012). The components of CC include chondrules, calcium-aluminum-rich inclusions (CAIs), fine-grained rim (FGR), and matrix material (Zega, 2004). Most chondrites have experienced secondary alteration, which resulted in the change of their primary texture, mineralogy, and chemical and isotopic compositions (Marrocchi et al., 2014). After establishing a new meteorite classification based on the secondary features, it appeared that petrologic type 3 is the most primitive type of meteorite, that petrologic types 2 and 1 may be the products of an increasing degree of aqueous alteration on the type 3 meteorites, and petrologic types 4–6 were subjected to thermal metamorphism (Buseck & Hua, 1993; McSween, 1979a). The information about the time and origin of solar nebula, formation of chondrules and refractory inclusions and their duration, heating and accretion, history of thermal metamorphism, and aqueous alteration can be obtained by studying CC meteorites (Amelin et al., 2002; Rudraswami et al., 2019).

The Mighei-like (CM) chondrites account for ~25% of the CC falls and ~0.7% of the total officially recognized meteorites (Suttle et al., 2021; Verdier-Paoletti et al., 2016). They are water-bearing meteorites with ~9 wt% H_2O bound in phyllosilicates, and mainly consist of up to 20 vol % chondrules, 57–85 vol% matrix, 1–11 vol% inclusions, and 1–3 vol% opaque minerals and minor components (such as sulfides and carbonates) (Cloutis, Hudon, et al., 2011; Grossman & Olsen, 1974; McSween, 1979b; Rubin et al., 2007; Scott & Krot, 2014; Weisberg et al., 2006). Geochemically, previous studies suggested that the CM chondrites show fairly homogeneous bulk chemical compositions, characterized by: (1) moderate enrichment in refractory elements relative to Ivuna-like (CI) chondrites, (2) specific value of Ca/Mg, Fe/Mg, Cr/Mg, and Mn/Mg, (3) depletion in elements more volatile than Mg relative to CI chondrites, and (4) flat REE patterns (e.g., Marrocchi et al., 2014; Rubin et al., 2007; Wasson & Kallemeyn, 1988; Wlotzka et al., 1989). Mineralogically speaking, the CM chondrites have clearly recorded aqueous alteration by reactions between liquid water and silicate rock during their evolution history, witnessed by the presence of products of aqueous alteration such as serpentine-group phyllosilicates, saponite-group phyllosilicates, and tochilinite–cronstedtite intergrowths (TCIs; previously assigned as "poorly characterized phases," PCP) (Cloutis, Hudon, et al., 2011; Marrocchi et al., 2014; Zolensky & McSween, 1988). CM chondrites are identified as the largest group of hydrated meteorites varying from less altered (Paris [CM2]) to heavily altered (Moapa Valley [CM1]) (Hewins et al., 2014; King et al., 2017; Zolensky et al., 1997), and various methods to determine the petrologic subtypes and degree of aqueous alteration of CM chondrites have been proposed (e.g., Browning et al., 1991, 1996; McSween, 1979b; Rubin et al., 2007). Specifically, the scale proposed by Rubin et al. (2007) is widely adopted by numerous studies to classify CM chondrites (e.g., Hewins et al., 2014; Lentfort et al., 2021; Ray & Shukla, 2018), which assigned the least altered samples as subtype 2.6 and the most altered (previous classified as CM1) as subtype 2.0. Hereafter, less altered CM chondrites with petrologic subtypes from CM 2.7–3.0 have since been proposed (e.g., Hewins et al., 2014; Kimura et al., 2020; Lentfort et al., 2021; Marrocchi et al., 2014). However, most CM chondrites are breccias with clasts of different degrees of alteration (e.g., Hewins et al., 2014; Lentfort et al., 2021; Potin et al., 2020; Zolensky et al., 2014), which may result in different estimation of their aqueous alteration, depending on which of the thin sections of the same meteorite is used. Therefore, a petrologic range is more accurate for an individual meteorite than a single number (King, Russell, et al., 2019; Lentfort et al., 2021). Hanowski and Brearley (2001) also developed a scheme for the aqueous alteration of chondrule in CM chondrites, which was specifically divided into four types. It is ambiguous whether the aqueous alteration of CM chondrites occurs on the parent body or in the nebula, and that question still remains under debate. Based on the characteristics of CM chondrites such as the bulk compositional homogeneity, the elemental exchange between chondrules and matrix during progressive alteration, and the occurrence of crosscutting dolomite veins, most studies hold the view that the aqueous alteration of CM chondrites occurred in situ on the parent body or bodies (e.g., Barber, 1981; Brearley, 2006; Browning et al., 1996, 2000; Jilly et al., 2014; Lee et al., 2016; McSween, 1979b), although some other works suggested that it occurred in the solar nebula (e.g., Grossman & Larimer, 1974; Metzler et al., 1992).

CM chondrites are an important meteorite group to understand the evolution of the early solar system. For example, CM-like clasts widely exist in many other meteorite groups such as howardite–eucrite–diogenite (HEDs), ureilites, ordinary chondrites, and so on (e.g., Briani et al., 2012; Fodor & Keil, 1976; Patzek et al., 2018; Zolensky & Ivanov, 2003; Zolensky et al., 1992, 1996), which has a great importance for understanding the dynamics of material transport and planetary accretion in the early solar system. However, clasts from other meteorite groups rarely occur in CM chondrites. To date, only three xenolithic fragments have been reported, including a white clast in the meteorite Murchison (Isa et al., 2014; Kerraouch et al., 2019), an igneous fragment in Northwest Africa (NWA) 12651 (Ebert et al., 2019), and a metamorphosed lithic clast in Grove Mountains (GRV) 021536 (Zhang et al., 2010). CM chondrite parent bodies are thought to have contributed to the delivery

of volatiles and organic material to the early Earth (Alexander et al., 2018; Cloutis et al., 2018; Gounelle et al., 2005; Langbroek et al., 2019). In addition, other chondrite groups or cometary material may also contribute to the volatile abundances in the solid Earth (Deligny et al., 2021). More recently, however, ECs were also considered as a possible material to deliver volatiles and organic material to the early Earth (Gray et al., 2021; Piani et al., 2020). Among these materials, it was previously suggested that CM chondrites may represent the type of material sampled by the ongoing OSIRIS-REx mission targeting B-type asteroid (101955) Bennu which is suspected to be dominated by hydrated clay-bearing minerals (phyllosilicates) and magnetite, indicating aqueous alteration (Clark et al., 2011; Hamilton et al., 2019; Lantz et al., 2018; Lauretta, 2014). However, recent study suggests that the samples returned from the asteroid Ryugu are similar to CI CCs but not CM chondrites (Yokoyama et al., 2022). Both Bennu and Ryugu are rubble-piled asteroids (Michel et al., 2020) and considered to be members of either the Polana or the Eulalia collisional families, which may originate from a common source in the main asteroid belt (Bottke et al., 2015; Campins et al., 2010; Simon et al., 2020; Sugita et al., 2019).

There are over 500 CM chondrites that have been recognized; however, only 21 of them are falls. Due to the terrestrial weathering, most CM chondrite finds are modified or overprinted by the terrestrial environment. Shidian is the first CM chondrite fall in China, which is affected only slightly by the terrestrial environment and may provide a new chance to get critical information about mineral composition and aqueous alteration of its parent body, as well as provide valuable information about the samples returned from Bennu by the ongoing OSIRIS-REx mission. Therefore, in order to classify and characterize Shidian meteorite, petrological, mineralogical, and geochemical studies on which were conducted in this paper. One metamorphic clast and two nontypical CM clasts (type 1) were identified in Shidian. Furthermore, in order to figure out whether Shidian can be an analog for Bennu asteroid, reflectance spectra and density of Shidian were also measured.

MATERIALS AND METHODS

Meteorite Sample and Petrographic Observations

Shidian is a new meteorite which fell in Dapizhai and Chenjiazhai village, Shidian county, Yunnan, China, on November 27, 2017, at 14:30 local time. The fall of Shidian was witnessed by eight local villagers and collected by one of them on the same day (Fig. 1). The meteorite landed on the red clay soil and was stored in the drawer of the collector, then part of which was bought by a meteorite hunter. The sample in this study was donated by the hunter, and was stored in a drying cabinet before further processing. The meteorite consists of two parts that are both covered by fusion crust and characterized by a black interior, with abundant white clasts (Fig. 1). In addition, the two fragments of the meteorite weighed 235 g (E 99°4′29.20″, N 24°41′54.81″) and 1574 g (E 99°4′41.92″, N 24°42′27.54″), respectively. The larger part of Shidian was sliced by a diamond wire cutting machine (STX-603A), and one larger piece (#1) was further processed as a polished thick section for analysis. Considering that most of the CM chondrites are heavily brecciated, another 11 relatively small pieces (numbers from #2 to #13) from the larger fragment were also processed as a single polished thick section for analysis. Each thick section was coated with a thin layer of carbon for petrographic observations, which were carried out by an FEI-Scios field emission scanning electron microscope (FE-SEM) equipped with an EDAX energy-dispersive detection system (EDS) at the Institute of Geochemistry, Chinese Academy of Sciences (IGCAS), with 15–30 kV accelerating voltage and 0.8–1.6 nA current. Modal abundances of minerals were estimated by ImageJ software on backscattered electron (BSE) images and elemental X-ray mapping images. The smallest grain size included in the estimate of modal mineral abundances is 2 μm.

Mineral Compositions

The mineral compositions of forsterite, fayalitic olivine, clinopyroxene, phyllosilicates in chondrules mesostasis and FGR, serpentine in matrix, and TCIs were determined with JXA 8230 electron microprobe analysis (EMPA) at Guilin University of Technology (GUT) and the State Key Laboratory of Ore Deposit Geochemistry, Institute of Geochemistry, Chinese Academy of Sciences. The chemical composition of fayalitic olivine, high-Ca pyroxene, nepheline, and plagioclase of the metamorphic clast were measured with JXA 8230 EMPA at GUT, and that of Cr-spinel from the metamorphic clast were measured with JXA 8530 EMPA at University of Science and Technology of China. The measurement was operated at an accelerating voltage of 15 kV, an electron beam current of 20 nA, and 1–10 μm diameter. Natural silicates were selected as standard, specifically, olivine for Mg, Ni, and Fe; plagioclase for Si, Ca, and Al; pyrope garnet for Mn, Cr, and Ti; kaersutite for Na; apatite for P; biotite for K; $ZnWO_4$ for Zn; and anhydride for S. The standard ZAF-correction procedure was used for data reduction. The detection limits of Na_2O, SiO_2, MgO, Al_2O_3, K_2O, CaO, and SO_3 were all 0.01%; FeO, MnO,

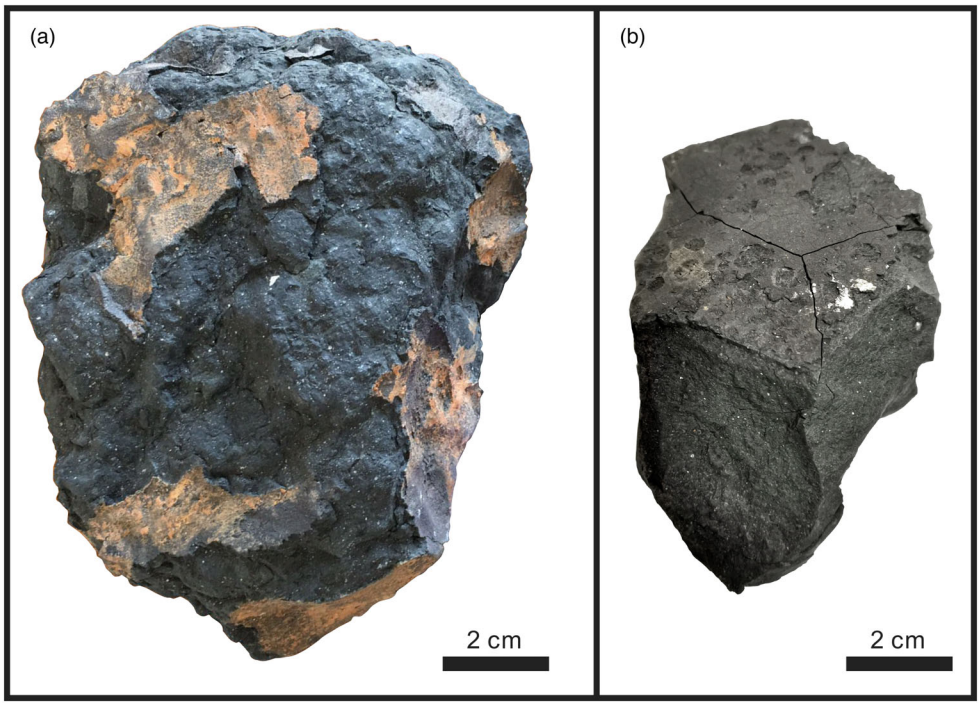

Fig. 1. a) The largest fragment of Shidian. b) The smaller fragment of Shidian. (Color figure can be viewed at wileyonlinelibrary.com.)

and P_2O_5 were 0.02%; NiO, Cr_2O_3, TiO_2 were 0.03%. The analytical errors were ~0.1 wt% for most elements. Phyllosilicates are too fine-grained to allow individual minerals to be analyzed; therefore, 10 μm probe diameter was applied for the determination of phyllosilicate representative bulk compositions (Rubin et al., 2007). A few measurements were excluded from the average calculation of the TCI compositions due to contamination with surrounding phases, which include measurements with >3.0 wt% Ni (perhaps from pentlandite or metal) and CaO >3.0 wt% (may be due to abundant calcite) (Lentfort et al., 2021).

Whole Rock Major and Trace Elements

Whole rock elemental concentrations were measured at the Guizhou Tongwei Analytical Technology Co. Ltd. Samples were crushed in an agate mortar with a pestle, then the pieces without white clasts were chosen for further analysis. An aliquot of a 50 mg whole rock sample of Shidian free of metamorphosed clast was digested with a double-distilled concentrated HNO_3-HF (1:4) mixture in a Teflon bomb for elemental concentration measurement. The solution was placed in an oven at 185 °C for 72 h. Residual sample was redigested with double-distilled concentrated HNO_3 followed by 2 N HNO_3. The solution was then dried and dissolved in 3 ml 2 N HNO_3 stock solution, which was then diluted to 1/4000 by 2% HNO_3 together with the addition of 10 ppb ^{61}Ni, 6 ppb Rh, In, and Re internal spikes. Finally, a Thermal X series 2 inductively coupled plasma mass spectrometer (ICP-MS) equipped with a Cetac ASX-510 Autosampler was used for measuring the elemental concentration.

Whole Rock Oxygen and Chromium Isotopic Composition

Whole rock oxygen isotopic composition of Shidian was determined at the University of New Mexico. Fresh fragments of interior materials weighing 4.2, 4.6, and 4.7 mg were selected under a stereomicroscope to avoid any possible contamination from fusion crust. Oxygen isotope analyses were performed using a CO_2 laser + BrF_5 fluorination system following modified procedures of Sharp (1990).

Oxygen isotopic compositions were reported using standard δ notation, and the $\delta^{17,18}O$ values have been calculated as $\delta^{17,18}O = ([^{17,18}O/^{16}O]_{sample}/[^{17,18}O/^{16}O]_{ref.} - 1) \times 10^3$ (‰), where the reference is the Vienna Standard Mean Ocean Water (V-SMOW). Thereafter, the $\delta^{17,18}O'$ values were calculated as $\delta^{17,18}O' = \ln(\delta^{17,18}O/1000 + 1) \times 1000$. The $\Delta^{17}O'$ values, which represent the deviation from the terrestrial fractionation line, have been obtained from the δ′ values following

$\Delta^{17}O' = \delta^{17}O' - 0.528 \times \delta^{18}O'$ in order to compare our results with those of previous studies. The analytical precision of a San Carlos olivine internal standard in this laboratory using the laser fluorination technique is ±0.004‰ for $\Delta^{17}O'$, which represents less than ±0.02‰ for the samples (Cano et al., 2020).

Whole rock chromium isotopic composition of Shidian was measured at the University of California Davis. Bulk powder of Shidian was generated by crushing a fusion crust–free chip using an agate mortar and pestle. Approximately 20 mg of the powder was used for the Cr isotopic measurements. The processing of bulk powder followed the procedure of Li et al. (2018). The separation of Cr from the bulk sample matrix was conducted using a three-column chemistry procedure reported by Yamakawa et al. (2009). The high-precision isotopic ratio determination of the purified Cr fractions was measured by a Thermo Triton Plus thermal ionization mass spectrometer following the procedure of Li et al. (2018). The Cr separate from sample was mixed with a silica gel-Al-boric acid activator and loaded onto four previously outgassed W filaments, with 3 μg Cr in each filament (total 12 μg). The four sample filaments were bracketed by a total of four filaments (two before, two after) and each of them loaded with 3 μg of the SRM 979 Cr standard. There are 1200 ratios (8 s integration time for each ratio) for each filament analysis, and the gain calibrations were made at the start of an analysis. After each block of 25 ratios, the background was measured and the amplifiers rotated. The $^{54}Cr/^{52}Cr$ ratios are expressed in ε-notation ($\varepsilon^{53,54}Cr = [(^{53,54}Cr/^{52}Cr)_{sample}/(^{53,54}Cr/^{52}Cr)_{SRM\ 979} - 1] \times 10^4$). (The 2SE errors shown in Table 5 include both the error from the sample as well as from the bracketing standard.)

Reflectance Spectrum

Samples used in this study were all stored in a dry environment at ~25 °C before processing. The visible and near-infrared (VIS–NIR) and infrared (IR) spectral signals were all collected from the fresh sections of chips, which are separated from a bulk sample. The samples used for the two measurements (wavelength from 0.35 to 2.5 μm, and from 2 to 16 μm) are not the same chip. The VIS–NIR reflectance spectra (wavelength from 0.35 to 2.5 μm) of Shidian were measured by the ASD FieldSpec4 spectrometer at the Reflectance Spectroscopy Laboratory of Shandong University in Weihai, Shandong Province, China. This spectrometer is equipped with a silicon array detector and two indium gallium arsenide detectors (InGaAs). A spectralon Diffuse Reflectance Standard white plate was employed to calibrate the measured spectra into reflectance as described in Zhang et al. (2020). The spectral measurement was performed with a phase angle of 30° (incident angle 0°, emission angle 30°) in ambient atmospheric environment. The temperature of sample surface illuminated by the spectrometer light source was about 40 °C.

The reflectance spectra of Shidian and Murchison (wavelength from 2 to 16 μm) were measured at Shanghai Institute of Technical Physics, Chinese Academy of Sciences, by a model 102F FT-IR spectrometer. The measurements were carried out in a thermostat filled with nitrogen at about 20 °C. A halogen lamp was used as light source. The Infragold calibration panel was measured before the measurement of each sample. Each sample was rotated by an angle of 90° after each measurement; therefore, four measured spectra and an average spectrum were acquired. The gold calibration panel was measured again after each measurement of a sample. The reflectance of the samples was calibrated by corresponding spectra of Infragold calibration panel.

Measurements of Grain Density, Bulk Density, and Porosity

The grain density, bulk density, and porosity of Shidian and Murchison were determined by the Micro-Ultrapyc 5000 ideal gas pycnometer following the method described by Li et al. (2012, 2019), which is briefly as follows. First, the mass of samples (m) was measured by a balance. Second, the grain volume of samples (V_g) was measured directly by the pycnometer, and the grain density (ρ_g) was calculated as $\rho_g = m/V_g$. Third, samples were loaded in the thin-wall balloon, which was subsequently evacuated, and the total volume (V_t) was determined by the pycnometer. Finally, the thin balloon was stripped from the sample, and the related volume (V_b) of bulk was obtained by the pycnometer. Therefore, the bulk volume of sample could be expressed as $V_t - V_b$, and the bulk density of which could be calculated as $\rho_b = m/(V_t - V_b)$ and the porosity as $P = (V_t - V_g)/V_t \times 100\%$.

RESULT

Petrography and Mineralogy of Shidian

Shidian consists of well-defined chondrules (~16–20 vol%) and fine-grained matrix (~80–84 vol%) with no clasts observed in sections #1, #4, #6, #9, #10, and #12. However, chondritic clasts in sections (#2, #3, #5, #7, #8, and #11) can be distinguished by the visible contrast between TCIs and the surrounding materials, and a metamorphosed clast can be observed in section #13, all of which are marked in Fig. 2. The meteorite

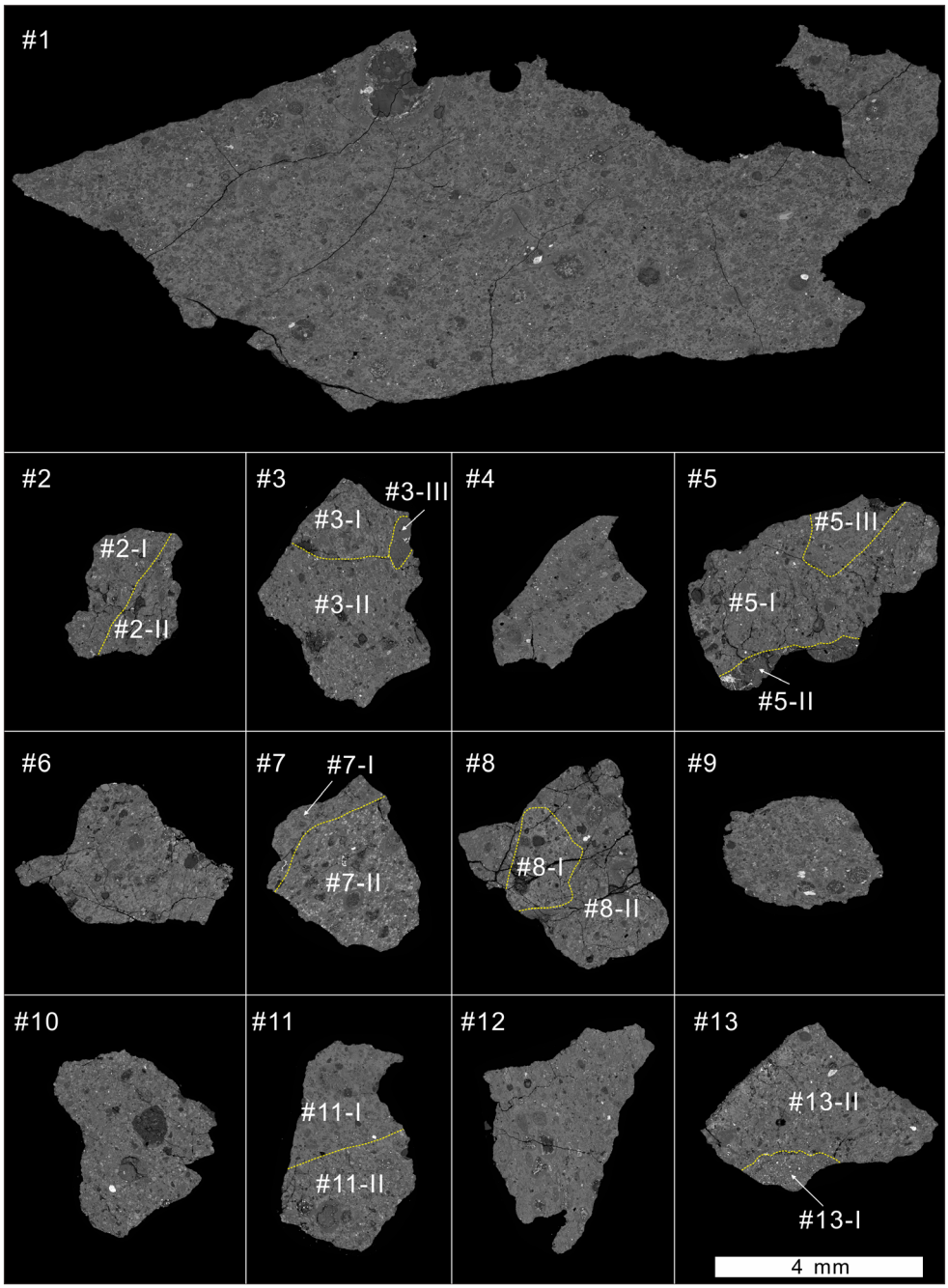

Fig. 2. The representative backscattered electron (BSE) image of polished thin sections of the Shidian meteorite. Clast with different aqueous alteration degree has been marked. The clast boundaries were determined by the different visible contrast between TCIs and the surrounding materials in different clasts.

main body and chondritic clasts mainly consist of forsterite (~13 vol%), fayalitic olivine (5 vol%), high-Ca pyroxene (2 vol%), phyllosilicates (~70 vol%), carbonates (~5 vol%), sulfide (~3 vol%), magnetite framboids (~2 vol%), and Fe-Ni metal (~0.2 vol%) (Figs. 2 and 3). The diameter of chondrules mainly varies from 100 to 1300 μm, with an average diameter of ~250 μm (Fig. 2). The chondrules mainly consist of olivine, serpentine vein, and irregular troilite, which are mainly of type I (Mg-rich, FeO-poor) and characterized by porphyritic textures; they are encompassed by compact FGRs (Fig. 3a, 3c, 3d and 3h). The mafic minerals in most chondrules have been partially altered and the mesostasis has been replaced by phyllosilicates

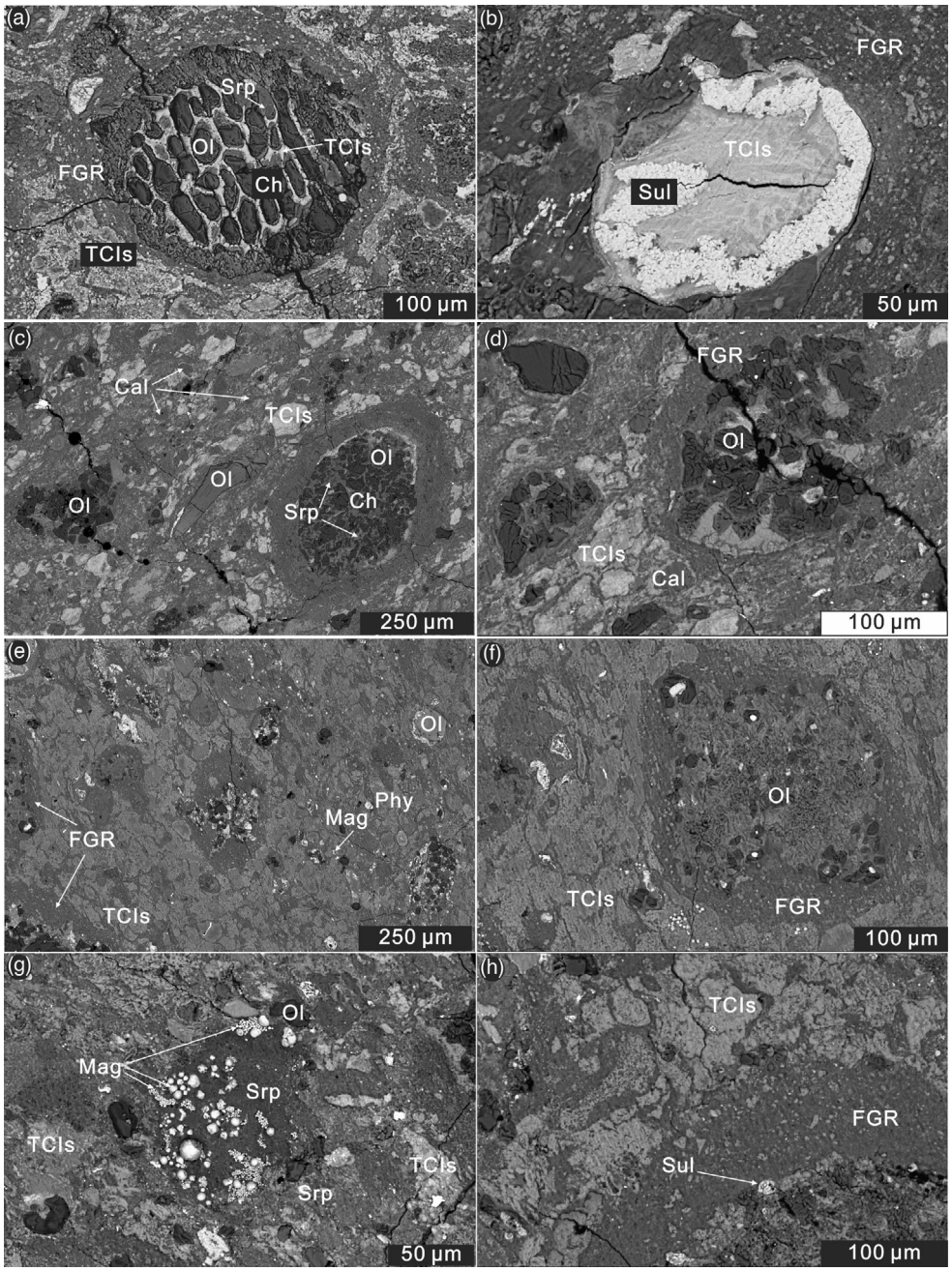

Fig. 3. a, b) BSE image of representative chondrule and sulfide in Section #1 of Shidian. c, d) BSE image of the representative area in Section #7. e, f) BSE image of the representative area in Section #12. g, h) BSE image of the representative area in Section #11. Ch = chondrules, FGR = fine-grained rim, Srp = serpentine, Ol = olivine, Phy = phyllosilicate, Px = pyroxene, Mag = magnetite, Sul = sulfide, Cal = calcite.

(Fig. 3a, 3c–e and 3f). Specifically, the mafic minerals in chondrules in #7-II fragment are minorly altered; however, the chondrules in clast #12 have been nearly completely replaced by the alteration products (Figs. 2 and 3c–f). The FGRs mainly consist of phyllosilicates and sulfide (Fig. 3h). The fine-grained matrix of Shidian mainly consists of phyllosilicates and isolated mineral grains including granular olivine, calcite, magnetite framboids, and sulfide (Fig. 3c–g). Additionally, most of the sulfide has been partially altered (Fig. 3b).

The metamorphosed clast (#13-I) has the sharp boundary with the Shidian host meteorite (#13-II) and mainly consists of olivine (~65 vol%), Ca-pyroxene

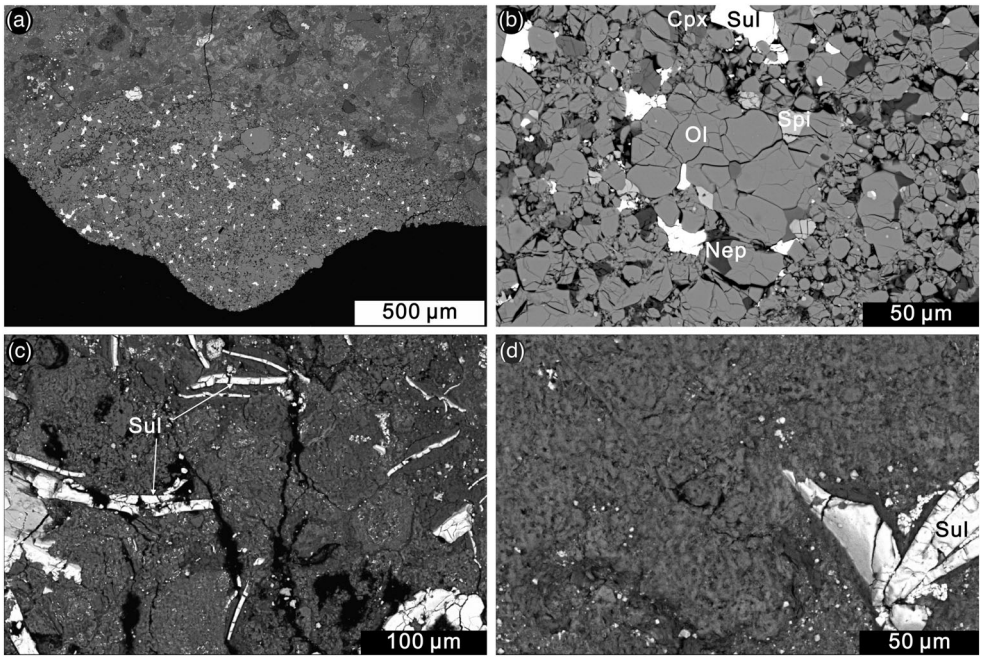

Fig. 4. a, b) BSE images of the metamorphosed clast (#13-I) of Shidian. c, d) BSE images of the clasts #5-II and #3-III of Shidian, respectively. Ol = olivine, Cpx = clinopyroxene, Nph = nepheline, Spl = spinel, Sul = sulfide.

Table 1. EMPA analysis mean composition (wt%) of olivine and high-Ca pyroxene in Shidian.

	CM clasts			#13-I clast				
	Forsterite (n = 11)	Fayalite (n = 25)	High-Ca pyroxene (n = 5)	Fayalite (n = 15)	High-Ca pyroxene (n = 15)	Nepheline (n = 12)	Plagioclase (n = 2)	Cr-spinel (n = 5)
K_2O	b.d.	b.d.	b.d.	n.a.	b.d.	1.14 ± 0.06	0.01 ± 0.02	n.a.
CaO	0.43 ± 0.18	0.19 ± 0.11	20.13 ± 1.45	0.39 ± 0.06	22.60 ± 0.42	2.81 ± 0.17	10.33 ± 0.18	0.06 ± 0.06
Al_2O_3	0.21 ± 0.16	0.04 ± 0.03	3.93 ± 2.14	0.03 ± 0.04	2.69 ± 0.82	33.92 ± 0.39	28.62 ± 0.65	27.63 ± 1.59
SiO_2	42.14 ± 0.47	37.24 ± 1.65	51.92 ± 3.04	36.09 ± 0.34	52.46 ± 1.10	43.25 ± 0.49	53.77 ± 0.49	0.21 ± 0.26
Cr_2O_3	0.13 ± 0.11	0.35 ± 0.09	1.59 ± 0.94	0.05 ± 0.05	0.65 ± 0.11	0.02 ± 0.02	0.04 ± 0.00	25.26 ± 1.47
MnO	0.02 ± 0.04	0.27 ± 0.07	0.35 ± 0.24	0.32 ± 0.06	0.09 ± 0.03	0.02 ± 0.03	b.d.	0.24 ± 0.03
Na_2O	0.01 ± 0.01	0.01 ± 0.01	0.01 ± 0.01	n.a.	0.60 ± 0.05	17.27 ± 0.37	5.62 ± 0.18	0.01 ± 0.01
MgO	56.84 ± 0.43	32.77 ± 6.72	20.14 ± 0.10	27.18 ± 0.45	13.37 ± 0.44	0.07 ± 0.05	0.13 ± 0.14	4.53 ± 0.19
TiO_2	0.07 ± 0.04	0.02 ± 0.02	0.88 ± 0.28	0.04 ± 0.04	0.66 ± 0.23	0.04 ± 0.07	0.06 ± 0.03	2.41 ± 0.46
FeO	0.52 ± 0.17	28.74 ± 8.16	1.00 ± 0.21	34.44 ± 0.37	6.99 ± 0.26	1.12 ± 0.12	1.13 ± 0.39	37.58 ± 0.46
NiO	0.02 ± 0.02	0.08 ± 0.05	0.05 ± 0.03	0.19 ± 0.05	0.08 ± 0.04	b.d.	b.d.	0.17 ± 0.01
P_2O_5	b.d.	n.a.	n.a.	n.a.	n.a.	0.01 ± 0.02	0.02 ± 0.01	n.a.
ZnO	0.02 ± 0.03	n.a.	n.a.	n.a.	n.a.	n.a.	n.a.	n.a.
V_2O_3	0.01 ± 0.02	n.a.	n.a.	n.a.	n.a.	n.a.	n.a.	n.a.
CoO	n.a.	n.a.	n.a.	0.10 ± 0.03	0.02 ± 0.01	b.d.	b.d.	0.16 ± 0.02
Total	100.44 ± 0.80	99.70 ± 0.73	100.00 ± 1.53	98.83 ± 0.72	100.21 ± 0.91	99.66 ± 0.83	99.74 ± 0.99	98.80 ± 0.39
Fo	99.5 ± 0.2	66.6 ± 10.9	n.g.	58.5 ± 0.5	n.g.	n.g.	n.g.	n.g.
Fa	0.5 ± 0.2	33.4 ± 10.9	n.g.	41.6 ± 0.5	n.g.	n.g.	n.g.	n.g.
Fs	n.g.	n.g.	1.6 ± 0.4	n.g.	11.7 ± 0.4	n.g.	n.g.	n.g.
Wo	n.g.	n.g.	41.1 ± 1.9	n.g.	48.4 ± 1.1	n.g.	n.g.	n.g.
An	n.g.	n.g.	n.g.	n.g.	n.g.	n.g.	50.3 ± 0.3	n.g.
Ab	n.g.	n.g.	n.g.	n.g.	n.g.	n.g.	49.6 ± 0.4	n.g.
$Fe^{3+}/\Sigma Fe$	n.g.	n.g.	n.g.	n.g.	n.g.	n.g.	n.g.	0.33 ± 0.02

b.d. = below detection limit; n.a. = not analyzed; n.g. = not given.

Table 2. EMPA analysis mean composition (wt%) of phyllosilicates in different clasts of Shidian.

Clast	#2-I (TCIs) (n = 12)	#2-II (TCIs) (n = 9)	#3-I (TCIs) (n = 8)	#3-II (TCIs) (n = 8)	#3-III (matrix) (n = 10)	#4 (TCIs) (n = 5)	#5-I (TCIs) (n = 9)	#5-II (matrix) (n = 9)
SiO_2	18.92 ± 4.01	21.38 ± 1.69	25.12 ± 1.33	22.08 ± 2.66	34.36 ± 0.95	26.81 ± 3.93	20.84 ± 4.91	34.72 ± 2.15
Al_2O_3	2.36 ± 0.51	2.73 ± 0.26	2.70 ± 0.11	2.65 ± 0.24	2.54 ± 0.39	2.61 ± 0.55	2.45 ± 0.67	3.17 ± 0.91
TiO_2	0.05 ± 0.03	0.04 ± 0.02	0.07 ± 0.03	0.03 ± 0.02	0.08 ± 0.04	0.06 ± 0.04	0.05 ± 0.04	0.03 ± 0.03
Cr_2O_3	0.21 ± 0.07	0.21 ± 0.04	0.17 ± 0.04	0.17 ± 0.06	0.16 ± 0.15	0.32 ± 0.14	0.21 ± 0.10	0.57 ± 0.25
FeO	42.85 ± 4.27	39.91 ± 3.41	40.10 ± 2.06	38.14 ± 2.77	23.30 ± 2.93	31.60 ± 7.33	42.27 ± 5.03	17.90 ± 4.23
MnO	0.18 ± 0.03	0.20 ± 0.04	0.20 ± 0.03	0.19 ± 0.03	0.19 ± 0.04	0.20 ± 0.03	0.19 ± 0.03	0.20 ± 0.07
MgO	11.17 ± 2.49	13.19 ± 2.36	12.40 ± 1.07	13.34 ± 2.35	21.89 ± 1.73	17.77 ± 4.72	11.32 ± 2.17	24.53 ± 3.73
CaO	0.15 ± 0.04	0.27 ± 0.06	0.22 ± 0.10	0.17 ± 0.07	0.11 ± 0.04	0.62 ± 0.62	0.32 ± 0.26	0.34 ± 0.24
Na_2O	0.37 ± 0.13	0.26 ± 0.04	0.29 ± 0.05	0.52 ± 0.09	0.10 ± 0.04	0.54 ± 0.09	0.30 ± 0.09	0.14 ± 0.04
P_2O_5	0.02 ± 0.03	0.01 ± 0.01	0.05 ± 0.05	0.01 ± 0.02	b.d.	0.09 ± 0.12	0.06 ± 0.16	0.04 ± 0.11
S	6.05 ± 2.83	4.53 ± 1.65	2.24 ± 0.48	5.33 ± 1.87	0.14 ± 0.12	3.16 ± 1.14	4.43 ± 2.17	0.59 ± 0.46
Ni	1.25 ± 0.50	0.97 ± 0.28	0.76 ± 0.31	1.18 ± 0.35	0.15 ± 0.14	0.67 ± 0.19	1.23 ± 0.39	0.67 ± 0.52
Total	83.60 ± 1.59	83.73 ± 1.08	84.38 ± 0.72	83.88 ± 1.77	83.03 ± 1.00	84.50 ± 1.81	83.71 ± 1.71	82.94 ± 2.34
S/SiO_2	0.37 ± 0.26	0.22 ± 0.09	0.09 ± 0.02	0.25 ± 0.11	n.g.	0.12 ± 0.05	0.25 ± 0.19	0.02 ± 0.01
FeO/SiO_2	2.42 ± 0.86	1.88 ± 0.25	1.60 ± 0.16	1.76 ± 0.29	0.68 ± 0.10	1.22 ± 0.40	2.20 ± 0.81	0.52 ± 0.15
Subtype	2.5	2.4	2.2	2.3	n.g.	2.2	2.5	n.g.

Clast	#5-III (TCIs) (n = 8)	#6 (TCIs) (n = 6)	#7-I (TCIs) (n = 8)	#7-II (TCIs) (n = 6)	#8-I (TCIs) (n = 8)	#8-II (TCIs) (n = 8)	#9 (TCIs) (n = 9)	#10 (TCIs) (n = 5)
SiO_2	26.77 ± 3.13	22.29 ± 2.91	23.95 ± 1.57	14.33 ± 2.63	20.26 ± 2.67	18.03 ± 4.70	23.96 ± 1.73	20.02 ± 3.97
Al_2O_3	2.60 ± 0.61	2.43 ± 0.66	2.45 ± 0.46	1.91 ± 0.28	3.06 ± 0.79	2.80 ± 0.69	2.49 ± 0.42	2.61 ± 0.69
TiO_2	0.02 ± 0.01	0.04 ± 0.06	0.05 ± 0.03	0.04 ± 0.03	0.03 ± 0.02	0.05 ± 0.03	0.03 ± 0.06	0.05 ± 0.04
Cr_2O_3	0.21 ± 0.06	0.27 ± 0.09	0.16 ± 0.06	0.20 ± 0.11	0.11 ± 0.05	0.26 ± 0.12	0.29 ± 0.09	0.20 ± 0.02
FeO	32.09 ± 7.94	37.58 ± 1.86	35.28 ± 4.28	45.84 ± 1.86	48.04 ± 4.50	40.48 ± 4.21	34.23 ± 4.66	39.49 ± 6.04
MnO	0.20 ± 0.03	0.21 ± 0.03	0.21 ± 0.03	0.16 ± 0.02	0.15 ± 0.03	0.18 ± 0.02	0.20 ± 0.05	0.22 ± 0.02
MgO	17.44 ± 5.76	14.09 ± 1.63	15.88 ± 2.84	9.78 ± 0.79	7.69 ± 2.77	12.53 ± 2.34	15.45 ± 3.00	13.51 ± 4.43
CaO	0.35 ± 0.55	0.16 ± 0.04	0.22 ± 0.04	0.09 ± 0.04	0.09 ± 0.03	0.18 ± 0.10	0.82 ± 1.01	0.19 ± 0.07
Na_2O	0.49 ± 0.08	0.32 ± 0.14	0.49 ± 0.12	0.15 ± 0.09	0.20 ± 0.08	0.42 ± 0.20	0.66 ± 0.12	0.36 ± 0.13
P_2O_5	0.03 ± 0.03	b.d.	0.01 ± 0.01	b.d.	b.d.	0.01 ± 0.01	0.10 ± 0.14	0.02 ± 0.05
S	2.39 ± 1.04	5.59 ± 1.94	4.64 ± 1.48	9.62 ± 1.79	2.69 ± 2.21	6.88 ± 2.68	4.30 ± 1.35	5.97 ± 2.66
Ni	0.76 ± 0.33	1.27 ± 0.44	1.19 ± 0.34	2.09 ± 0.27	0.36 ± 0.16	1.61 ± 0.62	1.28 ± 0.71	1.52 ± 0.61
Total	83.39 ± 1.71	84.30 ± 0.72	84.58 ± 1.00	84.24 ± 2.20	82.69 ± 1.53	83.46 ± 1.73	83.87 ± 1.81	84.20 ± 1.84
S/SiO_2	0.09 ± 0.03	0.26 ± 0.12	0.19 ± 0.06	0.70 ± 0.22	0.15 ± 0.13	0.45 ± 0.32	0.18 ± 0.06	0.33 ± 0.22
FeO/SiO_2	1.24 ± 0.43	1.72 ± 0.29	1.49 ± 0.26	3.29 ± 0.60	2.43 ± 0.51	2.48 ± 1.04	1.45 ± 0.30	2.10 ± 0.82
Subtype	2.2	2.3	2.2	2.6	2.5	2.5	2.2	2.5

Clast	#11-I (TCIs) (n = 11)	#11-II (TCIs) (n = 12)	#12 (TCIs) (n = 9)	FGR (n = 14)	Ser-matrix (n = 11)	Chondrule mesostasis (n = 11)
SiO_2	25.95 ± 0.79	19.41 ± 2.92	27.06 ± 2.14	33.37 ± 2.22	32.98 ± 3.94	29.58 ± 5.16
Al_2O_3	2.87 ± 0.37	2.45 ± 0.56	2.48 ± 0.26	2.50 ± 0.51	2.07 ± 0.34	2.39 ± 1.06
TiO_2	0.04 ± 0.02	0.03 ± 0.02	0.04 ± 0.05	0.06 ± 0.05	0.03 ± 0.02	0.16 ± 0.35
Cr_2O_3	0.35 ± 0.07	0.22 ± 0.07	0.20 ± 0.07	0.61 ± 0.14	0.24 ± 0.20	0.54 ± 0.31
FeO	36.22 ± 1.90	40.62 ± 3.67	31.67 ± 2.38	21.69 ± 2.22	21.45 ± 6.23	22.50 ± 5.11
MnO	0.21 ± 0.02	0.19 ± 0.03	0.23 ± 0.03	0.24 ± 0.06	0.22 ± 0.02	0.17 ± 0.03
MgO	14.08 ± 0.69	12.45 ± 1.59	17.36 ± 2.13	19.87 ± 1.75	24.54 ± 4.25	23.96 ± 3.86
CaO	0.39 ± 0.47	0.18 ± 0.07	0.34 ± 0.29	0.81 ± 0.61	0.27 ± 0.28	1.04 ± 1.74
Na_2O	0.36 ± 0.09	0.35 ± 0.13	0.59 ± 0.04	0.84 ± 0.09	0.50 ± 0.14	0.51 ± 0.22
P_2O_5	0.19 ± 0.33	0.01 ± 0.01	0.03 ± 0.05	0.13 ± 0.22	0.01 ± 0.02	b.d.
S	1.46 ± 0.67	6.61 ± 1.73	3.90 ± 1.74	2.85 ± 0.92	2.57 ± 1.38	5.02 ± 2.66
Ni	0.53 ± 0.48	1.72 ± 0.40	0.93 ± 0.37	1.69 ± 0.60	0.53 ± 0.44	0.46 ± 0.43
Total	82.70 ± 1.97	84.28 ± 1.20	84.96 ± 1.18	84.75 ± 1.53	85.46 ± 1.13	86.40 ± 1.90

Table 2. *Continued.* EMPA analysis mean composition (wt%) of phyllosilicates in different clasts of Shidian.

Clast	#11-I (TCIs) (n = 11)	#11-II (TCIs) (n = 12)	#12 (TCIs) (n = 9)	FGR (n = 14)	Ser-matrix (n = 11)	Chondrule mesostasis (n = 11)
S/SiO_2	0.06 ± 0.03	0.36 ± 0.16	0.15 ± 0.07	0.09 ± 0.03	0.08 ± 0.05	0.19 ± 0.12
FeO/SiO_2	1.40 ± 0.09	2.16 ± 0.53	1.18 ± 0.15	0.66 ± 0.10	0.68 ± 0.31	0.81 ± 0.31
Subtype	2.2	2.5	2.1	n.g.	n.g.	n.g.

b.d. = below detection limit; the subtype classification scenario proposed by Rubin et al. (2007) then extended by Lentfort et al. (2021) was adopted here.

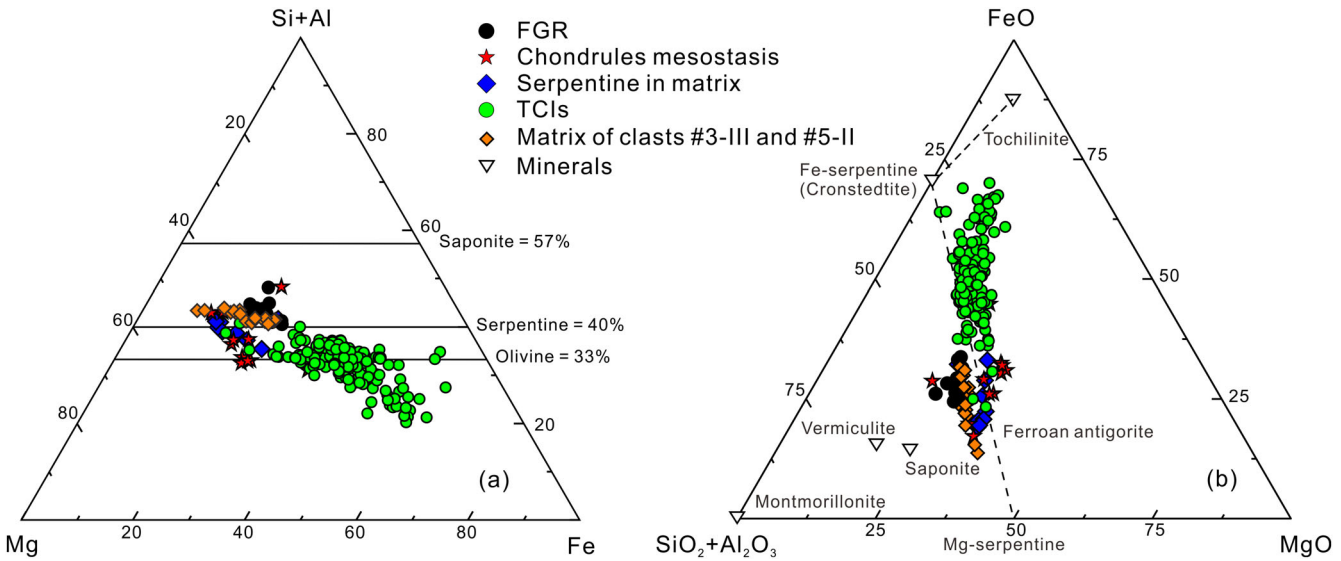

Fig. 5. a) Ternary diagram (atom%) of FGR, chondrule mesostasis, serpentine in matrix, matrix of clasts #3-III and #5-II, and TCIs. b) $SiO_2 + Al_2O_3$-FeO-MgO diagram (wt%) of FGR, chondrule mesostasis, serpentine in matrix, matrix of clasts #3-III and #5-II, and TCIs in Shidian, as well as some alteration minerals as Mg-serpentine, Fe-serpentine (cronstedtite), ferroan antigorite, montmorillonite, vermiculite, saponite from Takir et al. (2013). Tochilinite data are from Tomeoka and Buseck (1985). The phyllosilicate compositions lie along an approximately linear trend from near the composition of tochilinite (representing the least altered material) to the compositions that overshoot the serpentine solid solution line (representing the most altered material). (Color figure can be viewed at wileyonlinelibrary.com.)

(~14 vol%), nepheline and plagioclase (~15 vol%), Cr-spinel (~2%), and sulfides (~5 vol%, including pentlandite, troilite, and pyrrhotite) (Fig. 4a and 4b). Cr-spinel is generally developed near or within olivine as grains or inclusions, respectively. Two clasts (#3-III and #5-II) with lithofacies different from typical CM chondrites have also been identified (Fig. 4c and 4d). These two clasts mainly consist of serpentine and sulfide laths, with no anhydrous silicate observed.

Mineral Compositions

Electron microprobe analyses (EMPA) data for olivine and high-Ca pyroxene in Shidian are given in Table 1. It shows that the forsterite content (Fo) of Mg-rich olivine in Shidian varies from 99.1 to 99.7 mole% (avg. = 99.5 ± 0.2 mole%) among the 11 analyzed grains and the forsterite content (Fo) of Fe-rich olivine ranges from 40.5 to 83.5 mole% (avg. = 66.6 ± 10.9 mole%) among the 25 analyzed grains (Table 1). The ferrosilite content (Fs) and wollastonite content (Wo) of high-Ca pyroxene in Shidian vary from 1.1 to 2.0 mole% (Fs = 1.6 ± 0.4 mole%) and 39.2 to 44.0 mole% (Wo = 41.1 ± 1.9 mole%) among the five analyzed grains, respectively (Table 1). The composition of olivine and high-Ca pyroxene from #13-I clast is equilibrated, with the fayalite content (Fa) varying from 40.3 to 42.6 mole% (Fa = 41.6 ± 0.5 mole%) among the 15 analyzed olivine grains, the ferrosilite content (Fs) and wollastonite content (Wo) varying from 11.1 to 12.5 mole% (Fs = 11.7 ± 0.4 mole%), and 46.1 to 50.1 mole% (Wo = 48.4 ± 1.1 mole%) among the 15 analyzed high-Ca pyroxene grains, respectively (Table 1). The NiO and CaO content in olivine from

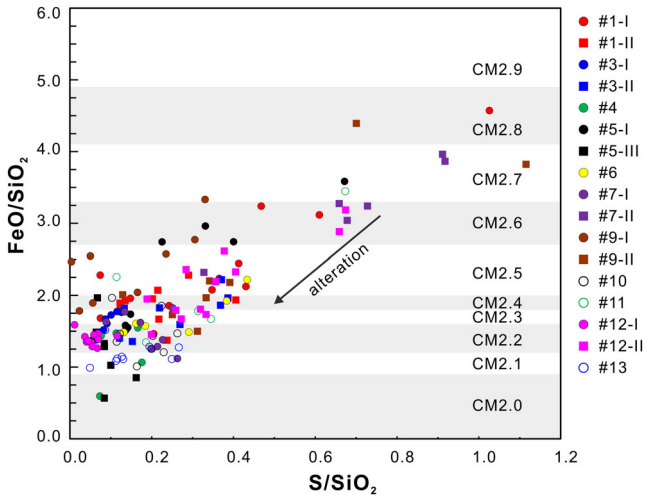

Fig. 6. FeO/SiO_2 versus S/SiO_2 ratios of TCIs in different clast of Shidian. The alteration trend and threshold value of FeO/SiO_2 were distinguished by Lentfort et al. (2021), indicating that the "FeO" and "S" content of fluid decreases when increasing the aqueous alteration. (Color figure can be viewed at wileyonlinelibrary.com.)

#13-I clast are 0.19 ± 0.05 wt% and 0.39 ± 0.06 wt%, respectively, and the TiO_2 content in spinel from #13-I clast is 2.41 ± 0.46 wt% (Table 1).

The mineral composition of phyllosilicate in FGR, chondrule mesostasis, matrix of clasts #3-III and #5-II, TCIs, and serpentine in matrix has also been determined, and analytical totals vary from 77.63 to 91.02 wt% (avg. = 84.07 ± 1.75 wt%), showing a typical range for total masses for serpentine and saponite in chondrites (Table 2) (Zolensky et al., 1993). Selected elements of serpentine in matrix, FGR, chondrule mesostasis, matrix of clasts #3-III and #5-II, and TCIs were plotted in ternary diagrams, which showed that these phyllosilicates lie along an approximately linear trend that extends from the Fe endmember (tochilinite or magnetite) toward the Mg-serpentine; in addition, phyllosilicates in FGR and chondrule mesostasis, serpentine in matrix, and parts of TCIs all locate near the serpentine line (Fig. 5) (Nakamura, 2006; Takir et al., 2013). Regarding SiO_2 in TCIs, it ranges from 10.64 to 33.51 wt%, clast #7-II having the lowest mean SiO_2 content (SiO_2 = 14.33 ± 2.63 wt%) and highest mean FeO/SiO_2 (3.29 ± 0.60), while clast #12 has the highest mean SiO_2 content (SiO_2 = 27.06 ± 2.14 wt%) and the lowest mean FeO/SiO_2 (1.18 ± 0.15) (Table 2). As to other clasts, the mean FeO/SiO_2 ratio of clast #3-I, #4, #5-III, #7–1, #9, and #11–1 ranges from 1.22 to 1.60, that of clasts #3-II and #6 ranges from 1.72 to 1.76, that of clast #2-II is 1.88, that of clasts #2-I, #5-I, #8-I, #8-II, #10, and #11-II varies from 2.10 to 2.48 (Table 2). Furthermore, a positive correlation between the FeO/SiO_2 and S/SiO_2 ratio of TCIs has been identified in different clasts of Shidian (Fig. 6).

Bulk Chemistry

The whole rock major and trace element compositions of Shidian are reported in Table 3. The meteorite is characterized by Fe_2O_3 of 28.5 wt%, CaO of 1.64 wt%, and MgO of 19.1 wt%. Selected major and trace elements were plotted for comparison with other CM chondrites (such as Sutter's Mill, Paris, Jbilet Winselwan, and Aguas Zarcas), sorted from left to right as a function of their condensation temperature (Tc) (50% decrease) (Fig. 7a) (Kiseeva & Wood, 2015; Lodders, 2003). Compared to CI chondrites, Shidian is depleted in highly volatile elements (e.g., Ga, Cs, Zn, and Sn), but enriched in refractory elements and moderately volatile elements (Fig. 7a). The Sc/Mn × 1000 (at) and Zn/Mn × 100 (at) of Shidian are 5.7 and 8.6, respectively. The rare earth element abundance of Shidian is higher than that of CI chondrites and approximately 1.5 × CI chondrite. The CI chondrite normalized (after Lodders, 2003) rare earth element pattern of Shidian is flat with an $(La/Yb)_N = 1.04$ (Fig. 7b).

Bulk Oxygen and Chromium Isotopic Composition

The bulk oxygen isotopic composition of Shidian (relative to V-SMOW, Lodders & Fegley, 1998) is shown in Table 4 and is plotted in the oxygen three isotope plot (Fig. 8) along with published oxygen isotopic composition of Paris and other CCs.

The oxygen isotopic composition of Shidian is characterized by $\delta^{17}O$ ranging from −1.32‰ to 0.10‰ (avg. = −0.51 ± 0.73‰), $\delta^{18}O$ ranging from 4.34‰ to 6.33‰ (avg. = 5.44 ± 1.01‰), and $\Delta^{17}O$ ranging from −3.61‰ to −3.24‰ (avg. = −3.38 ± 0.20‰).

The results of chromium isotopic analysis are shown in Table 5 and are plotted in Fig. 9 together with $\Delta^{17}O$ values. The determined $\varepsilon^{53}Cr$ of Shidian is 0.20 ± 0.03 and the $\varepsilon^{54}Cr$ is 1.00 ± 0.11 (Table 5).

Reflectance Spectrum Observations

The reflectance spectrum of Shidian between 0.4 and 2.5 μm was normalized at 0.55 μm and shown in Fig. 10a and 10c. Shidian displays absorption features at 0.765, 0.923, and 1.160 μm, which are characteristic absorption features of phyllosilicates in CM matrix (Fig. 10c) (Cloutis, Hudon, et al., 2011). Additionally, Shidian also displays absorption features at 1.780, 1.930, and 2.210 μm (Fig. 10c). Specifically, it is suggested that the 0.765 μm absorption feature is associated with the ferrous (Fe^{2+}) to ferric (Fe^{3+}) charge transfer common for oxidized iron in phyllosilicates (e.g., Vilas, 2008); the absorption at

Table 3. Whole rock chemical composition of Shidian.

Element	Concentration	Unit	Element	Concentration	Unit
Li	1.43	μg g^{-1}	Cs	0.12	μg g^{-1}
Be	0.03	μg g^{-1}	Ba	4.14	μg g^{-1}
Mg	11.5	wt%	La	0.34	μg g^{-1}
P	1080	μg g^{-1}	Ce	0.83	μg g^{-1}
Ca	1.17	wt%	Pr	0.13	μg g^{-1}
Sc	7.58	μg g^{-1}	Nd	0.64	μg g^{-1}
Ti	532	μg g^{-1}	Sm	0.21	μg g^{-1}
V	63.3	μg g^{-1}	Eu	0.08	μg g^{-1}
Cr	3140	μg g^{-1}	Gd	0.27	μg g^{-1}
Mn	1630	μg g^{-1}	Tb	0.05	μg g^{-1}
Fe	19.9	wt%	Dy	0.34	μg g^{-1}
Co	583	μg g^{-1}	Ho	0.07	μg g^{-1}
Ni	1.26	wt%	Er	0.21	μg g^{-1}
Cu	122	μg g^{-1}	Tm	0.03	μg g^{-1}
Zn	166	μg g^{-1}	Yb	0.23	μg g^{-1}
Ga	7.85	μg g^{-1}	Lu	0.03	μg g^{-1}
Rb	1.61	μg g^{-1}	Hf	0.14	μg g^{-1}
Sr	14.9	μg g^{-1}	Ta	0.02	μg g^{-1}
Y	1.98	μg g^{-1}	Pb	1.19	μg g^{-1}
Zr	4.99	μg g^{-1}	Th	0.04	μg g^{-1}
Nb	0.39	μg g^{-1}	U	0.01	μg g^{-1}
Mo	1.54	μg g^{-1}	Sc/Mn × 1000 (at)	5.68	n.g.
Sn	0.85	μg g^{-1}	Zn/Mn × 100 (at)	8.56	n.g.
Sb	0.09	μg g^{-1}	$(La/Yb)_N$	1.04	n.g.

The uncertainties of Na, Mg, K, Ca, Fe, Co, and Ni are lower than 0.1%; the uncertainties of trace elements are about 10%.

1.930 μm is the result of the presence of unbound water (molecule H_2O) (Aines & Rossman, 1984); the absorption at 2.210 μm is associated with the structural water in phyllosilicates (Cloutis, 1989; Hunt, 1979). The overall "blue" (negative) slope of Shidian reflectance spectrum between 0.4 μm and 2.5 μm resembles those of B-type asteroids and Bennu (Fig. 10a). Both Shidian meteorite and Ryugu asteroid have a shoulder at 0.5 μm, while the shoulder is absent for Bennu asteroid due to the wavelength range used in Fig. 10a. This shoulder is also observed in serpentine, which may associate with the ultraviolet absorption at <0.5 μm (Fe–O charge transfer) (Cloutis, Hiroi, et al., 2011). To compare the characteristics of reflectance spectrum between Shidian meteorite and asteroids, principal component analysis based on the method described in DeMeo et al. (2009) were conducted. Specifically, the fourth principal component (PC4′) of Shidian was calculated as 0.0639, which was plotted in Fig. 11 combined with $Slope_{0.85–1.8}$. To compare the reflectance spectrum between Shidian and boulders from Bennu, four bands of the multispectral Map-Cam imager (one of the three cameras in the OSIRIS-REx Camera Suite) were also used to calculate the band ratios and slope for Shidian, including b': 473 nm, v: 550 nm, w: 698 nm, and x: 847 nm (e.g., DellaGiustina et al., 2020). The spectral slope from b' to x was calculated as −0.328, which was plotted in Fig. 12 along with the near-UV index (b'/v).

The reflectance spectrum ranging from 2.3 to 3.4 μm for Shidian and Murchison was normalized to 2.4 μm, and the reflectance spectrum of asteroid Bennu, meteorites Ivuna, LAP 02277, MET 00639, and Cold Bokkeveld is also plotted for comparison (Fig. 10b). From this spectrum, one can see that Shidian and Murchison have a wide and strong absorption feature around 3 μm, which is attributed to hydroxyl- and/or water-bearing materials (e.g., Cloutis et al., 2018; Lebofsky, 1980; Sunshine et al., 2009; Takir et al., 2013). Specifically, the reflectance intensity of Shidian and Murchison dropped off significantly at 2.72–2.80 μm, which is attributed to phyllosilicate (Cloutis, Hiroi, et al., 2011). However, the ~3 μm absorption feature at Shidian and Murchison meteorites is broader than that in other CM chondrites and Bennu asteroid. The broad band in the meteorites is associated with water adsorbed in the meteorites from the Earth's atmosphere (Takir et al., 2013). In addition, a weak absorption feature at 3.4–3.5 μm is observed, attributed to C–H stretching of aliphatic organic compounds (Clark et al., 2009; Takir et al., 2013).

The Density and Porosity of Shidian and Murchison

The measured grain densities, bulk densities, and porosities of Shidian and Murchison are presented in

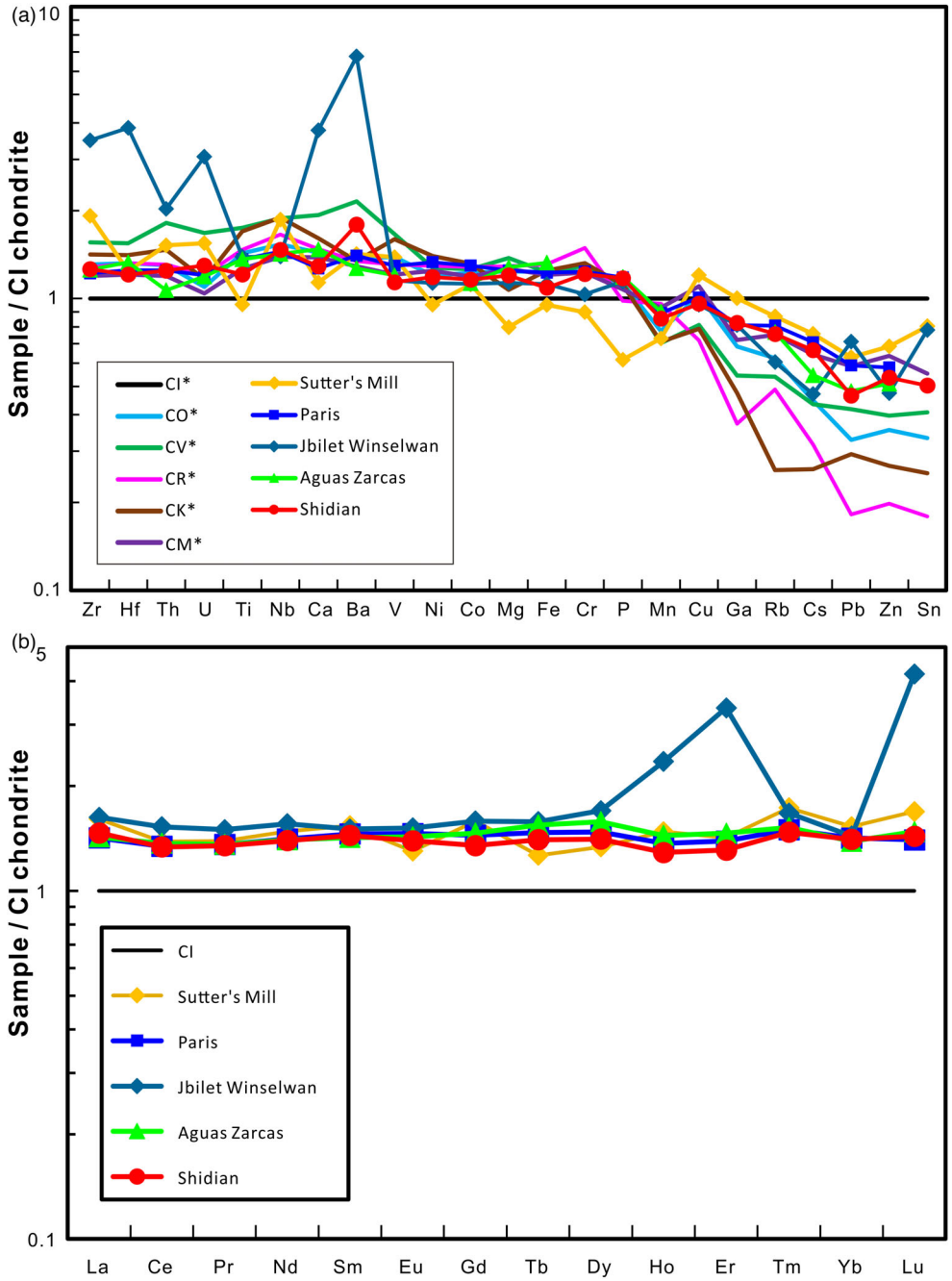

Fig. 7. Analysis of (a) selected trace elements spider diagram and (b) rare earth element spider diagram. The data of Paris are from Hewins et al. (2014), the data of Sutter's Mill are from Jenniskens et al. (2012), the data of Jbilet Winselwan are from King, Russell, et al. (2019), the data of Aguas Zarcas are from Kerraouch et al. (2022), the data of CI chondrite are from Lodders (2003), and the data of other chondrites are from Braukmüller et al. (2018). (Color figure can be viewed at wileyonlinelibrary.com.)

Table 6. The grain densities of Shidian and Murchison were measured as 2.758 ± 0.008 g cm^{-3} and 2.908 ± 0.002 g cm^{-3}, respectively. The determined bulk densities of Shidian and Murchison are 2.500 ± 0.004 g cm^{-3} and 2.383 ± 0.006 g cm^{-3}, respectively, with porosities calculated at $9.37 \pm 0.59\%$ and $18.06 \pm 0.02\%$, respectively.

DISCUSSION

Classification of Shidian

Although Shidian has been officially classified as CM2 chondrite (Meteoritical Bulletin Database, 108), new insights and evidence for its classification were

Table 4. Oxygen isotopic compositions of Shidian.

Sample	$\delta^{17}O$ (‰)	1σ	$\delta^{18}O$ (‰)	1σ	$\Delta^{17}O$ (‰)	1σ
Shidian	0.10		6.33		−3.24	
	−0.32		5.64		−3.29	
	−1.32		4.34		−3.61	
Average	−0.51	0.73	5.44	1.01	−3.38	0.20
Paris[a]	−2.11		2.43		−3.37	
	−1.43		4.40		−3.72	
	−0.37		6.14		−3.56	
	0.33		6.21		−2.91	
	0.75		6.80		−2.79	
	−1.15		4.09		−3.28	
	−1.87		3.63		−3.76	
	−2.15		3.44		−3.94	
	0.62		6.97		−3.00	
	−0.66		5.11		−3.31	
	−1.20		4.68		−3.63	
Average	−0.84	1.06	4.90	1.48	−3.39	0.37

$\Delta^{17}O$ calculated using the formula $\Delta^{17}O = \delta^{17}O' - 0.528 \times \delta^{18}O'$.
[a]Reported in Hewins et al. (2014).

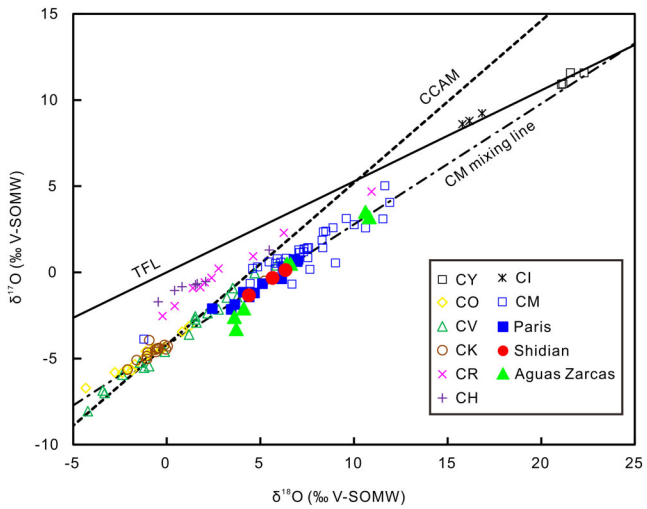

Fig. 8. Oxygen isotopic compositions of Shidian. Data for Shidian are from this study; for Paris are from Hewins et al. (2014); for Aguas Zarcas are from Kerraouch et al. (2021); and for other chondrites are from Clayton and Mayeda (1999), Moriarty et al. (2009), and King, Bates, et al. (2019). TFL refers to the terrestrial fractionation line. CCAM refers to the carbonaceous chondrite anhydrous minerals. CM mixing line is from Suttle et al. (2021). (Color figure can be viewed at wileyonlinelibrary.com.)

provided here. Petrologically, Shidian is a brecciated CM chondrite based on the extremely high abundance of fine matrix (~80–84 vol%), low abundance of Fe-Ni metal (0.2 vol%), relatively small chondrule size (~250 μm), and the presence of abundant phyllosilicates and clasts with different aqueous alteration degrees (Figs. 2 and 3) (e.g., Brearley & Jones, 1998; Cloutis, Hudon, et al., 2011; Friend et al., 2018; Hewins et al., 2014; Lentfort et al., 2021; McSween, 1979a; Rubin, 2010). Geochemically, Shidian has consistent characteristics with CM chondrites, including depletion in highly volatile elements (Fig. 7a), Sc/Mn × 1000 (at) = 5.7 and Zn/Mn × 100 (at) = 8.6 (Table 3), and a flat pattern of rare earth elements with $(La/Yb)_N = 1.04$ (Fig. 7b) (e.g., Friedrich et al., 2018; Hewins et al., 2014; Lee et al., 2019; Wasson & Kallemeyn, 1988). The bulk oxygen isotopic compositions of Shidian ($\delta^{17}O = -1.32‰$ to 0.10‰, $\delta^{18}O = 4.34‰$ to 6.33‰) correspond to most of the CM chondrites and some CV chondrites, and fall onto the CM mixing line (slope of ~0.7 and a $\delta^{17}O$ intercept of −4.23‰), therefore reflecting the mixing between two primitive reservoirs with an inner $\delta^{16}O$-rich solar-like silicate reservoir and an outer $\delta^{16}O$-poor component (Fig. 8) (e.g., Clayton & Mayeda, 1999; Hewins et al., 2014; Moriarty et al., 2009; Suttle et al., 2021; Tonui et al., 2014). Additionally, the oxygen and chromium isotopic compositions of Shidian correspond to a CC reservoir, more particularly characteristics of the CM chondrites and CV chondrites (Fig. 9) (e.g., Li et al., 2018; Sanborn & Yin, 2014; Sanborn et al., 2013; Sanborn, Yin, & Irving, 2014; Sanborn, Yin, Rumble, et al., 2014; Schmitz et al., 2016; Warren, 2011a, 2011b; Yin et al., 2009).

Most CM chondrites have experienced a series of post-accretionary processes, which mainly include (i) brecciation, (ii) aqueous alteration, or (iii) post-alteration heating (Brearley, 2006; Lee et al., 2019). First, Shidian did not undergo significant thermal metamorphism, which is witnessed by the high average chromium content of fayalitic olivine (avg. = 0.35 ± 0.09 wt%) (Table 1), and the presence of a large amount of phyllosilicate with the low

Table 5. Chromium isotopic composition of Shidian.

Sample	Meteorite type	ε^{53}Cr (±2SE)[a]	ε^{54}Cr (±2SE)[a]
Shidian	CM	0.20 ± 0.03	1.00 ± 0.11
Diepenveen[b]	CM	0.13 ± 0.05	0.85 ± 0.10
Murchison[c]	CM	0.12 ± 0.04	0.89 ± 0.09
		0.01 ± 0.04	0.10 ± 0.15
JP-1[d]		0.03 ± 0.05	0.07 ± 0.09
		0.03 ± 0.03	0.03 ± 0.07

[a]ε^{54}Cr is a part per 10,000 deviation of $^{54}Cr/^{52}Cr$ ratio of the samples relative to SRM 979. The 2SE errors for these ratios correspond to ~16 sets of 300 ratios of the sample and the bracketing standard (only the ratio[s] outside the twice the population standard deviation was rejected at this stage). The error of the bracketing standard was then propagated to the error of each sample.
[b]Reported in Langbroek et al. (2019).
[c]Reported in Yin et al. (2009).
[d]Reported in Yamakawa and Yin (2014). JP-1 is an ultramafic geological reference material.

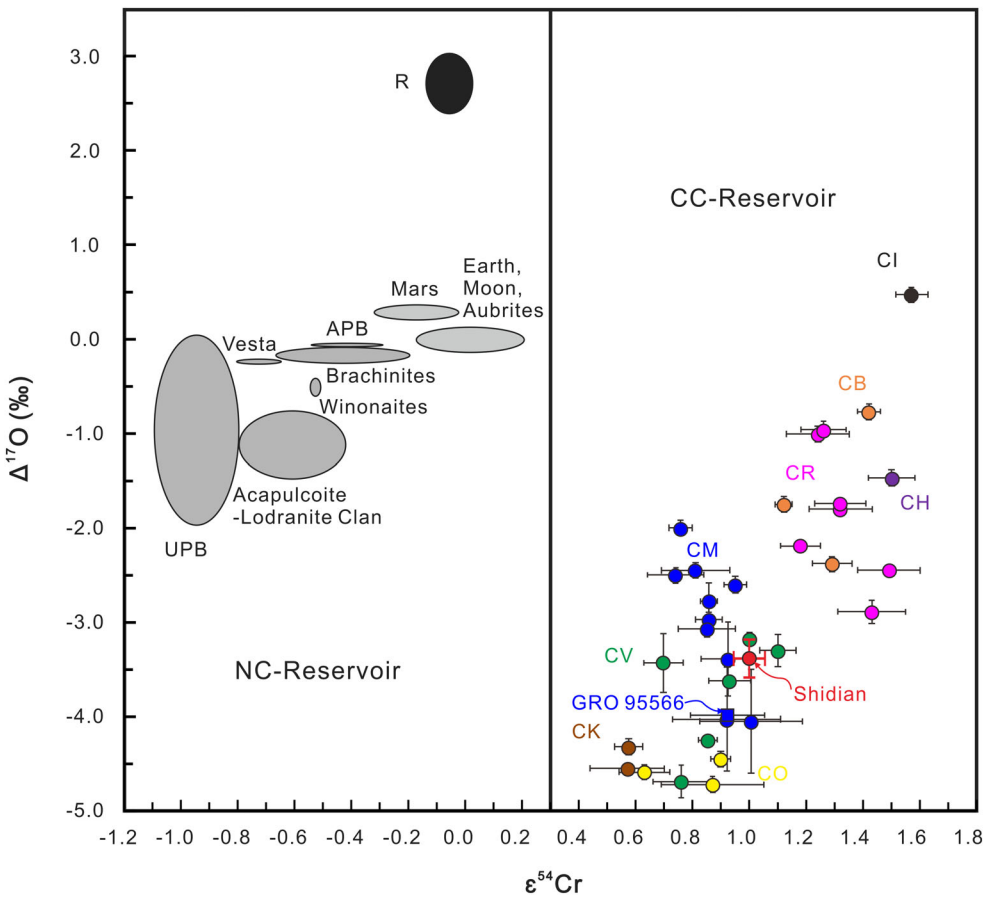

Fig. 9. $\Delta^{17}O$–$\varepsilon^{54}Cr$ composition of Shidian in comparison to other chondrite and achondrite meteorite groups. The template and data set are from Zhu et al. (2021) and references therein. The $\varepsilon^{54}Cr$ data for GRO 95566 (CM) are from Torrano et al. (2021), and the $\Delta^{17}O$ data for which are from Clayton and Mayeda (1999). (Color figure can be viewed at wileyonlinelibrary.com.)

EMPA analytical totals (avg. = 84.07 ± 1.75 wt%) (Table 2) (e.g., Alexander et al., 2012, 2013; Amsellem et al., 2020; Miyamoto, 1991; Ray & Shukla, 2018; Tonui et al., 2014; Velbel & Zolensky, 2021). Second, as other CM chondrites, aqueous alteration is the main post-accretionary processing of Shidian, during which abundant aqueous alteration products (such as phyllosilicate and carbonate) were generated (e.g., Lee & Ellen, 2008; Rubin et al., 2007). Finally, Shidian experienced a brecciation, which is witnessed by the chondritic clasts with different alteration degrees and the metamorphosed clast (Fig. 2) and may be the

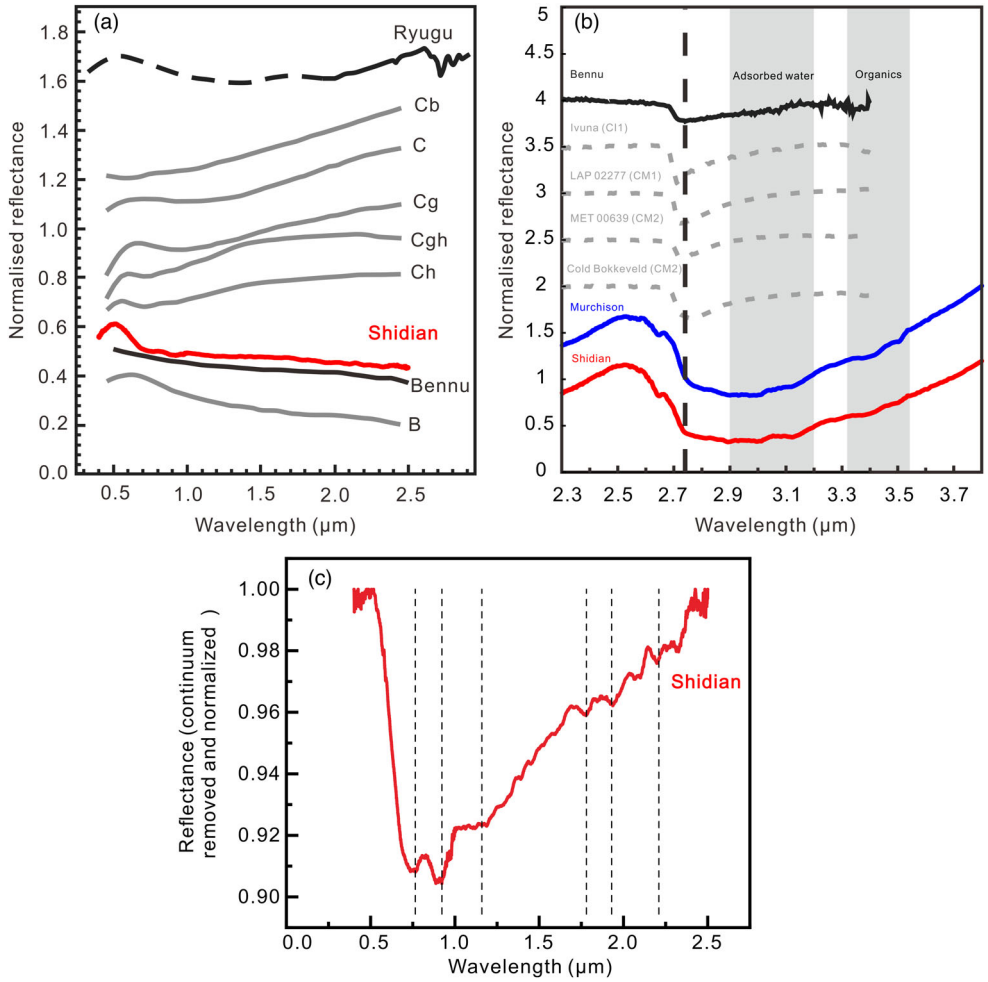

Fig. 10. a) Reflectance spectrum of Shidian (red line) and C-class asteroids in the range of 0.4–2.5 μm. The spectra have been normalized to unity at 0.55 μm. Normalized results are compared to the spectra of C-class asteroids, offset in steps of ±0.1 (DeMeo et al., 2009), and to the on-orbit (and ground-based, dashed) surface-averaged spectrum of Ryugu by Kitazato et al. (2019), offset by +0.7. The average whole-disk, full-rotation OVIRS spectrum of Bennu is from Hamilton et al. (2019). b) Reflectance spectrum of Shidian (red line) and Murchison (blue line) in the range of 2.3–3.4 μm. The spectra have been normalized to unity at 2.4 μm. Normalized results are compared to the spectra of CI chondrites, CM chondrites, and Bennu, all offset in steps of ±0.5 (Hamilton et al., 2019). The dotted vertical line at 2.74 μm denotes the Bennu band minimum position. The gray-shaded areas for adsorbed water and organics are from Takir et al. (2013). c) Reflectance spectrum of Shidian (red line) with continuum removed and normalized in the range of 0.4–2.5 μm. The dashed lines are characteristic absorption features. The data plotted in (a) and (c) are the same data, but the data plotted in (b) are not the same data as (a) and (c). (Color figure can be viewed at wileyonlinelibrary.com.)

result of multiple low-energy impacts (e.g., Alexander et al., 2013; Joy et al., 2020; Lindgren et al., 2015; Patzek et al., 2018; Suttle et al., 2021). Specifically, the anhydrous silicate in most chondritic clasts has been partially replaced by the alteration products, indicating clasts of type 2; however, the anhydrous silicate of chondrules in clasts #3-III and #5-II has been completely replaced by the alteration products with the residual chondrules displaying pseudomorphic outlines, hence indicating a clast of type 1 (e.g., Suttle et al., 2021). Considering the clasts #3-III and #5-II are not typical CM lithofacies, therefore, Shidian is a type 2 brecciated CM chondrite.

Scale of the Aqueous Alteration of Shidian

It is suggested that the composition of secondary phases in CM chondrite was controlled by the composition of alteration fluid but not the composition of the host phase being replaced (Velbel et al., 2012, 2015). For example, the composition of alteration fluid is characterized by Fe-rich and S-rich in early stage, but Mg-rich, S-poor in late stage, which is recorded by the aqueous alteration products (such as phyllosilicate and carbonate) (Hanowski & Brearley, 2001; Suttle et al., 2021; Velbel et al., 2012). A positive correlation between the FeO/SiO_2 and S/SiO_2 ratios in Shidian was

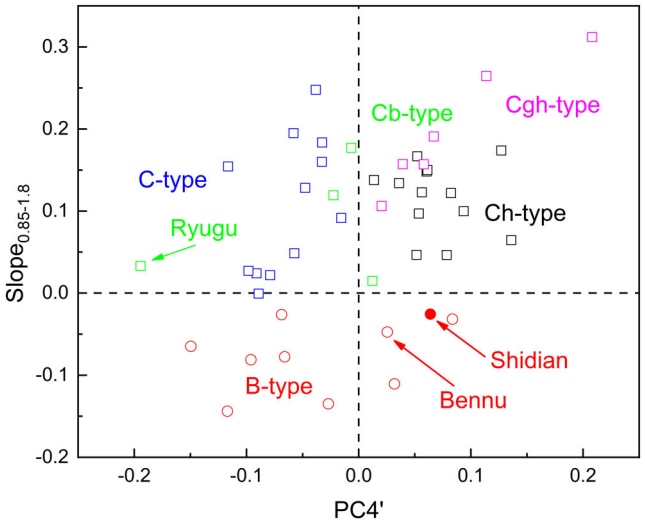

Fig. 11. $Slope_{0.85–1.8}$ versus PC4′ of Shidian and some asteroids. The $Slope_{0.85–1.8}$ is the ratio of reflectance at 1.8 μm to that at 0.75 μm, and the PC4′ (fourth principal component) is calculated by the asteroid taxonomy online tool from the MIT web (http://smass.mit.edu/busdemeoclass.html) according to DeMeo et al. (2009). The data of asteroids were collected from Zhang et al. (2022) and references therein. (Color figure can be viewed at wileyonlinelibrary.com.)

identified (Fig. 6), which was also previously reported in other CM chondrites and indicates that the "FeO" and "S" content of fluid decreases when increasing the aqueous alteration (e.g., Lentfort et al., 2021). In other words, the composition of phyllosilicate in CM chondrite is a proxy for the degree of aqueous alteration.

Based on the chemistry of phyllosilicates in Shidian, we suggest that serpentine in matrix, chondrule mesostasis, and FGR should be the later alteration products, while the TCIs should be the early alteration product (Fig. 5). Although Shidian has not undergone thermal metamorphism, it has experienced brecciation; thus, the aqueous alteration classification scenario proposed by Rubin et al. (2007) with a single subtype number for individual meteorites is not applicable to Shidian. Therefore, the extended scenario reported by Lentfort et al. (2021) was adopted here, which assigned the number range for the individual brecciated CM chondrites mainly based on the FeO/SiO_2 of TCIs. Specifically, in BSE images, TCIs in most clasts are gray (e.g., clasts #2-I, #2-II, and #10), and that in clast #12 is dark gray, while that in clasts #7-II is light gray; the contrast between TCIs and surroundings in clasts #3-I, #4, #5-III, #7-I, #9, #11-I, and #12 is lower than others. With the combination of the FeO/SiO_2 ratios of each clast, Shidian was classified as CM 2.1–2.6 subtype, and dominantly as CM 2.2 subtype (Fig. 6).

Origin of the Metamorphosed Clast

The clast (#13-I) of Shidian is characterized by a well-recrystallized texture and by a compositional equilibrated olivine and pyroxene, which implies that this clast experienced a strong thermal metamorphism. Olivine grains in #13-I clast have low Cr_2O_3 content (0.05 ± 0.05 wt%) and high CaO content (0.39 ± 0.06 wt%), which also implies a strong thermal metamorphism (e.g., Grossman, 2004; Kerraouch et al., 2019). Based on the olivine/Cr-spinel geothermometers proposed by Wlotzka (2005), which was modified from that in Fabriès (1979) for the application of most chondrites, the equilibrium temperature of the clast (#13-I) was calculated as 798 ± 24 °C. The clast is characterized by low abundance of Fe-Ni metal and high Fa content of olivine, which indicates that this clast was generated in an oxidizing environment (e.g., Kerraouch et al., 2019). The absence of low-Ca pyroxene may be the result of its replacement by high-Ca pyroxene under oxidizing conditions with ferroan olivine, and Na-Ca-rich feldspathic mesostasis co-crystallized, which has been observed in some CCs (CO3, CR2, and CM2) (e.g., Jogo et al., 2013).

Rumuruti (R) chondrites have Fa values consistent with the clast (#13-I); however, the clast (#13-I) should not be an R-chondritic fragment because this clast has lower NiO content (0.19 ± 0.05 wt%) and higher CaO content (0.39 ± 0.06 wt%) in olivine, and lower TiO_2 content (2.41 ± 0.46 wt%) in spinel than R chondrites (e.g., Bischoff et al., 2011; Kerraouch et al., 2019; Zhang et al., 2010). The mineral assemblage and composition of clast (#13-I) in Shidian are consistent with that of the white clast from Murchison and metamorphosed clast from GRV 021536 (e.g., Kerraouch et al., 2019; Zhang et al., 2010), which may indicate a similar source for both of them. These clasts may originate from the depth within CV chondrite parent body by partial melting or within the CM chondrite parent body by fluid-assisted percolation during metasomatism (e.g., Kerraouch et al., 2019; Zhang et al., 2010). Data from this paper are insufficient to figure out whether this clast (#13-I) is a cognate or exotic clast. However, compared with these two clasts, clast (#13-I) has higher Fe^{3+} content in spinel, indicating that clast (#13-I) originated from a more oxidizing environment.

Potential Parent Asteroid of Shidian and Implication

The cosmic ray exposure (CRE) ages of most CM chondrites are shorter and lesser than 2 Ma with peaks at ~0.2 and ~0.6 Ma, which indicate that CM chondrites may be delivered from near-Earth asteroids

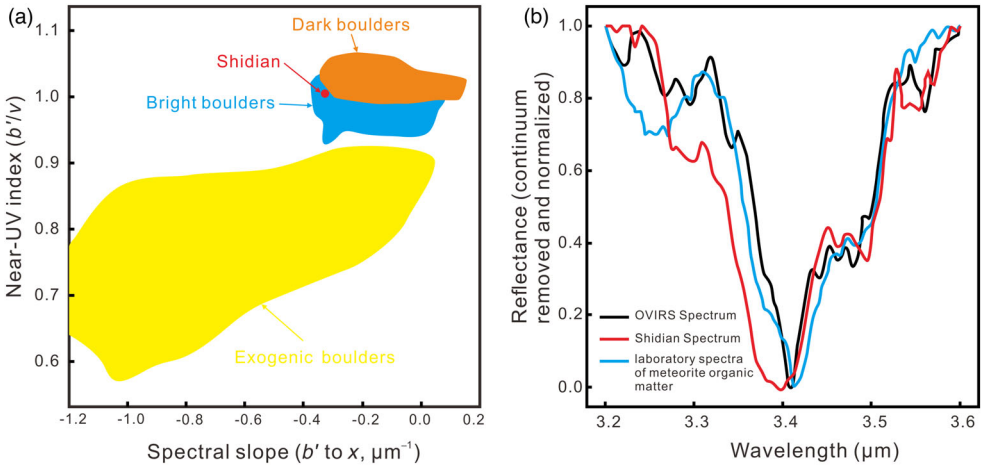

Fig. 12. a) Near-UV index (b'/v) versus spectral slope (b' to x, μm^{-1}) of Shidian and representative boulders on Bennu' surface. The data of bright and dark boulders are from DellaGiustina et al. (2020), and the data of exogenic boulders are from Tatsumi et al. (2021). The slope γ was calculated by the least square fitting with model that $R_{band} = 1 + \gamma\ (\lambda_{band} - 0.55\ \mu m)$ (band = b', v, w), where R_{band} is the v-band normalized reflectance and λ_{band} is the wavelength at the center of the band filter in microns (e.g., Tatsumi et al., 2021). b) Comparisons of the reflectance among Shidian, OVIRS spectrum of Bennu, and laboratory spectra of meteorite organic matter at 3.4 μm region. The OVIRS spectrum of Bennu and laboratory spectra of meteorite organic matter are from Kaplan et al. (2020). (Color figure can be viewed at wileyonlinelibrary.com.)

Table 6. Mass, volume, density, and porosity values of Shidian and Murchison.

Sample	Mass (g)	Grain volume (cm^3)	1SD	Bulk volume (cm^3)	1SD	Grain density (g cm^{-3})	1SD	Bulk density (g cm^{-3})	1SD	Porosity (%)	1SD
Shidian-1_1	5.546	2.011	0.006	2.208	0.004	2.758	0.008	2.511	0.004	8.95	0.02
Shidian-1_2	5.546	2.011	0.006	2.229	0.004	2.758	0.008	2.488	0.004	9.79	0.02
Shidian avg.						2.758	0.008	2.500	0.004	9.37	0.59
Murchison	7.039	2.421	0.002	2.955	0.008	2.908	0.002	2.383	0.006	18.06	0.02

(King et al., 2020; Nishiizumi et al., 2014; Nishiizumi & Caffee, 2009, 2012; Zolensky et al., 2020). However, it is suggested that CM chondrites may also be delivered from the Main Belt, which is deduced from the pre-atmospheric orbits for Sutter's Mill and Maribo (Borovička et al., 2019; Jenniskens et al., 2012). Previous studies suggest that the spectral characteristics of CM chondrites are similar to those of C-complex asteroids (Cloutis, Hudon, et al., 2011; DeMeo et al., 2009). For Shidian meteorite, the reflectance spectrum characteristics of which are corresponding to the B-type asteroid (such as [101955] Bennu). Specifically, the reflectance spectrum of Shidian meteorite shows a "blue" (negative) continuum slope across the visible and near-infrared wavelengths (may result from the presence of insoluble organic material and/or magnetite due to possible space weathering), which along with the near-infrared absorption at ~2.7 μm are similar to the B-type asteroid (e.g., Clark et al., 2011; Cloutis, Hiroi, et al., 2011; Cloutis, Hudon, et al., 2011; Hamilton et al., 2019; Thompson et al., 2019); the PC4′ and $Slope_{0.85–1.8}$ of the reflectance spectrum of Shidian meteorite is also consistent with Bennu asteroid (Fig. 11). Moreover, combining the bulk density of Bennu proposed by Chesley et al. (2014) and that of Shidian meteorite, the macroporosity of Bennu could be deduced as 49.6 ± 0.3%, which is consistent within its uncertainty with the previously reported value of 40 ± 10% (e.g., Chesley et al., 2014) and indicates that Shidian could be the candidate analog for Bennu.

Compared with the "boulders" recently found on Bennu, the reflectance spectrum characteristics across the visible and near-infrared wavelengths of Shidian correspond to the "bright boulders" (DellaGiustina et al., 2020). Additionally, the reflectance spectrum in the 3.4 μm region of Shidian is also similar to one of the OSIRIS-REx Visible and InfraRed Spectrometer (OVIRS) spectra from Bennu, which are consistent with the insoluble organic matter (Kaplan et al., 2020). The clast (#13-I) from Shidian contains pyroxene (~14 vol %), which may correspond to the pyroxene-bearing boulders distinguished by DellaGiustina et al. (2020).

The pyroxene-bearing boulders on Bennu were suggested to originate from a fragment of (4) Vesta by DellaGiustina et al. (2020), however, which is not so for the clast (#13-I) from Shidian due to the inconsistent mineral compositions between the clast (#13-I) and the HED meteorites. Although carbonates are found both in Shidian (Fig. 3h) and Bennu (e.g., Kaplan et al., 2020), their occurrence is inconsistent. Specifically, carbonates exist in the form of veins on Bennu but in the form of particles in Shidian, which may result from sample bias of Shidian or camera resolution of OVIRS. As an analog for Bennu, Shidian meteorite may provide valuable information about the samples returned of Bennu by the OSIRIS-REx mission, such as the mineralogy characteristics, the existence of organic materials, or the alteration degree, among others. Based on the truth that one metamorphic clast and two type 1 clasts with nontypical CM lithofacies were observed in Shidian, and the heterogeneous aqueous alteration degree of Shidian with the subtype from 2.1 to 2.6, we suggest that the samples returned by the OSIRIS-REx mission from Bennu may be characterized by heterogeneous aqueous alteration degree, containing the metamorphic clast not originated from Vesta and the type 1 clast with nontypical CM lithofacies.

CONCLUSION

Based on the petrologic, mineralogic, geochemical, spectral reflectance, and physical studies of Shidian, the following conclusions can be drawn.

1. Shidian is a breccia consisting of fine-grained matrix (~80 to 84 vol%) and type-IA chondrules (~16 to 20 vol%; ~250 μm). The mineralogy mainly consists of forsterite, fayalitic olivine, high-Ca pyroxene, phyllosilicates, sulfide, carbonates, magnetite framboids, or Fe-Ni metal, among others. Based on the combination of the petrology, major and trace elements, typical oxygen isotopic compositions, characteristic chromium isotopic compositions, and reflectance spectra, Shidian should be classified as a brecciated CM chondrite.
2. Shidian has experienced brecciation, aqueous alteration, but no evidence of heating. Clasts with different aqueous alteration degree were observed in Shidian. According to the classification scenario proposed by Rubin et al. (2007) and later extended by Lentfort et al. (2021), Shidian was classified as the CM 2.1–2.6 subtype. The metamorphosed clast (#13-I) has experienced a strong thermal metamorphism and was generated from an oxidizing environment; it should accrete into the CM chondrite after the aqueous alteration on the parent body of Shidian.
3. Shidian may be an analog for B-type asteroid (such as [101955] Bennu), which is supported by similar mineral composition (dominated by phyllosilicates), consistent reflectance spectrum ("blue" slope across the visible and near-infrared wavelengths), and suitable density and porosity. The characteristics of reflectance spectrum of Shidian correspond to the bright boulders on Bennu; in addition, carbonate and insoluble organic exist both in Shidian and Bennu. The petrological and mineral characteristics of Shidian indicate that the samples returned by the OSIRIS-REx mission from Bennu may be characterized by heterogeneous aqueous alteration degree, containing the type 1 nontypical CM lithofacies and the metamorphic clast not originated from Vesta.

Acknowledgments—This work was supported by the Strategic Priority Research Program of the Chinese Academy of Science, Grant NO. XDB41000000, the Chinese Academy of Sciences "Light of West China" Program (Shijie Li, 2019), Space Debris Project (KJSP2020020101), and the National Natural Science Foundation of China (Grants 42173046). The authors are grateful to Jincheng Lv for providing valuable meteorite sample and information about Shidian. We thank Dr. Lanfang Xie from the Guilin University of Technology for her assistance in the EMPA lab. We are grateful to the FIB laboratory team at IGCAS for the SEM observation and BSE image obtainment. We would like to express our gratitude to Dr. Edward Cloutis for editing the manuscript and for providing precious comments. We also thank Dr. Ashley King and Dr. Michael A. Velbel for their valuable comments that greatly improved this paper, and Dr. A. J. Timothy Jull for his help as editor.

Data Availability Statement—The data that support the findings of this study are openly available in Mendeley Data at https://doi.org/10.17632/wpdkxnh8cf.2.

Editorial Handling—Dr. Edward Anthony Cloutis

REFERENCES

Aines, R. D., and Rossman, G. R. 1984. Water in Minerals? A Peak in the Infrared. *Journal of Geophysical Research: Solid Earth* 89: 4059–71.

Alexander, C. M. O'D., Bowden, R., Fogel, M. L., Howard, K. T., Herd, C. D. K., and Nittler, L. R. 2012. The Provenances of Asteroids, and Their Contributions to the Volatile Inventories of the Terrestrial Planets. *Science* 337: 721–3.

Alexander, C. M. O'D., Howard, K. T., Bowden, R., and Fogel, M. L. 2013. The Classification of CM and CR Chondrites Using Bulk H, C and N Abundances and

Isotopic Compositions. *Geochimica et Cosmochimica Acta* 123: 244–60.
Alexander, C. M. O'D., McKeegan, K. D., and Altwegg, K. 2018. Water Reservoirs in Small Planetary Bodies: Meteorites, Asteroids and Comets. *Space Science Reviews* 214: 36–83.
Amelin, Y., Krot, A. N., Hutcheon, I. D., and Ulyanov, A. A. 2002. Lead Isotopic Ages of Chondrules and Calcium-Aluminum-Rich Inclusions. *Science* 297: 1678–83.
Amsellem, E., Moynier, F., Mahan, B., and Beck, P. 2020. Timing of Thermal Metamorphism in CM Chondrites: Implications for Ryugu and Bennu Future Sample Return. *Icarus* 339: 113593.
Barber, D. J. 1981. Matrix Phyllosilicates and Associated Minerals in C2M Carbonaceous Chondrites. *Geochimica et Cosmochimica Acta* 45: 945–70.
Bischoff, A., Vogel, N., and Roszjar, J. 2011. The Rumuruti Chondrite Group. *Geochemistry* 71: 101–33.
Borovička, J., Popova, O., and Spurný, P. 2019. The Maribo CM 2 Meteorite Fall—Survival of Weak Material at High Entry Speed. *Meteoritics & Planetary Science* 54: 1024–41.
Bottke, W. F., Vokrouhlický, D., Walsh, K. J., Delbo, M., Michel, P., Lauretta, D. S., Campins, H., Connolly, H. C., Jr., Scheeres, D. J., and Chelsey, S. R. 2015. In Search of the Source of Asteroid (101955) Bennu: Applications of the Stochastic YORP Model. *Icarus* 247: 191–217.
Braukmüller, N., Wombacher, F., Hezel, D. C., Escoube, R., and Münker, C. 2018. The Chemical Composition of Carbonaceous Chondrites: Implications for Volatile Element Depletion, Complementarity and Alteration. *Geochimica et Cosmochimica Acta* 239: 17–48.
Brearley, A. J. 2006. The Action of Water. In *Meteorites and the Early Solar System II*, edited by D. S. Lauretta and H. Y. McSween, 587–624. Tucson, Arizona: University of Arizona Press.
Brearley A. J., and Jones R. H. 1998. Chondritic Meteorites. In *Planetary Materials*, edited by J. J. Papike (Chapter 3). *Reviews in Mineralogy*, vol. 36. Washington, DC: Mineralogical Society of America.
Briani, G., Gounelle, M., Bourot-Denise, M., and Zolensky, M. E. 2012. Xenoliths and Microxenoliths in H Chondrites: Sampling the Zodiacal Cloud in the Asteroid Main Belt. *Meteoritics & Planetary Science* 47: 880–902.
Browning, L. B., McSween, H. Y., and Zolensky, M. E. 1996. Correlated Alteration Effects in CM Carbonaceous Chondrites. *Geochimica et Cosmochimica Acta* 60: 2621–33.
Browning, L. B., Mcsween, H. Y., and Zolensky, M. E. 2000. On the Origin of Rim Textures Surrounding Anhydrous Silicate Grains in CM Carbonaceous Chondrites. *Meteoritics & Planetary Science* 35: 1015–23.
Browning, L. B., Zolensky, M. E., and Barrett, R. 1991. Serpentine and Modal Compositions of CM Chondrites (Abstract #XXII). 22nd Lunar and Planetary Science Conference. CD-ROM.
Buseck, P. R., and Hua, X. 1993. Matrices of Carbonaceous Chondrite Meteorites. *Annual Review of Earth and Planetary Sciences* 21: 255–305.
Campins, H., Morbidelli, A., Tsiganis, K., De León, J., Licandro, J., and Lauretta, D. 2010. The Origin of Asteroid 101955 (1999 RQ36). *The Astrophysical Journal Letters* 721: L53–7.
Cano, E. J., Sharp, Z. D., and Shearer, C. K. 2020. Distinct Oxygen Isotope Compositions of the Earth and Moon. *Nature Geoscience* 13: 270–4.
Chesley, S. R., Farnocchia, D., Nolan, M. C., Vokrouhlický, D., Chodas, P. W., Milani, A., Spoto, F., et al. 2014. Orbit and Bulk Density of the OSIRIS-REx Target Asteroid (101955) Bennu. *Icarus* 235: 5–22.
Clark, B. E., Binzel, R. P., Howell, E. S., Cloutis, E. A., Ockert-Bell, M., Christensen, P., Barucci, M. A., et al. 2011. Asteroid (101955) 1999 RQ36: Spectroscopy from 0.4 to 2.4 mm and Meteorite Analogs. *Icarus* 216: 462–75.
Clark, R. N., Curchin, J. M., Hoefen, T. M., and Swayze, G. A. 2009. Reflectance Spectroscopy of Organic Compounds: 1 Alkanes. *Journal of Geophysical Research: Planets* 114: E3.
Clayton, R. N., and Mayeda, T. K. 1999. Oxygen Isotope Studies of Carbonaceous Chondrites. *Geochimica et Cosmochimica Acta* 63: 2089–104.
Cloutis, E. A. 1989. Spectral Reflectance Properties of Hydrocarbons: Remote-Sensing Implications. *Science* 245: 165–8.
Cloutis, E. A., Hiroi, T., Gaffey, M. J., Alexander, C. M. O'D., and Mann, P. 2011. Spectral Reflectance Properties of Carbonaceous Chondrites: 1 CI chondrites. *Icarus* 212: 180–209.
Cloutis, E. A., Hudon, P., Hiroi, T., Gaffey, M. J., and Mann, P. 2011. Spectral Reflectance Properties of Carbonaceous Chondrites: 2 CM Chondrites. *Icarus* 216: 309–46.
Cloutis, E. A., Pietrasz, V. B., Kiddell, C., Izawa, M. R., Vernazza, P., Burbine, T. H., DeMeo, F., et al. 2018. Spectral Reflectance "deconstruction" of the Murchison CM2 Carbonaceous Chondrite and Implications for Spectroscopic Investigations of Dark Asteroids. *Icarus* 305: 203–24.
Deligny, C., Füri, E., and Deloule, E. 2021. Origin and Timing of Volatile Delivery (N, H) to the Angrite Parent Body: Constraints from in situ Analyses of Melt Inclusions. *Geochimica et Cosmochimica Acta* 313: 243–56.
DellaGiustina, D. N., Burke, K. N., Walsh, K. J., Smith, P. H., Golish, D. R., Bierhaus, E. B., Ballouz, R.-L., et al. 2020. Variations in Color and Reflectance on the Surface of Asteroid (101955) Bennu. *Science* 370: eabc3660.
DeMeo, F. E., Binzel, R. P., Slivan, S. M., and Bus, S. J. 2009. An Extension of the Bus Asteroid Taxonomy into the Near-Infrared. *Icarus* 202: 160–80.
Dodd, R. T., Jr., Van Schmus, W. R., and Koffman, D. M. 1967. A Survey of the Unequilibrated Ordinary Chondrites. *Geochimica et Cosmochimica Acta* 31: 921–51.
Ebert, S., Patzek, M., Lentfort, S., and Bischoff, A. 2019. Accretion of Differentiated Achondritic and Aqueously Altered Chondritic Materials in the Early Solar System—Significance of an Igneous Fragment in the CM Chondrite NWA 12651. *Meteoritics & Planetary Science* 54: 2985–95.
Fabriès, J. 1979. Spinel-Olivine Geothermometry in Peridotites from Ultramafic Complexes. *Contributions to Mineralogy and Petrology* 69: 329–36.
Fodor, R. V., and Keil, K. 1976. Carbonaceous and Non-Carbonaceous Lithic Fragments in the Plainview, Texas, Chondrite: Origin and History. *Geochimica et Cosmochimica Acta* 40: 177–89.
Friedrich, J. M., Abreu, N. M., Wolf, S. F., Troiano, J. M., and Stanek, G. L. 2018. Redox-Influenced Trace Element Compositional Differences Among Variably Aqueously Altered CM Chondrites. *Geochimica et Cosmochimica Acta* 237: 1–17.
Friend, P., Hezel, D. C., Barrat, J. A., Zipfel, J., Palme, H., and Metzler, K. 2018. Composition, Petrology, and Chondrule-Matrix Complementarity of the Recently Discovered Jbilet Winselwan CM2 Chondrite. *Meteoritics & Planetary Science* 53: 2470–91.

Gounelle, M., Engrand, C., Alard, O., Bland, P. A., Zolensky, M. E., Russell, S. S., and Duprat, J. 2005. Hydrogen Isotopic Composition of Water from Fossil Micrometeorites in Howardites. *Geochimica et Cosmochimica Acta* 69: 3431–43.

Gray, M. L., Weisberg, M. K., Ebel, D. S., Alexander C. M. O'D., Foustoukos, D. I., and Howard, K. T. 2021. Abundances and Isotopic Compositions of Volatile H, N, C in Unequilibrated Enstatite Chondrites and the Volatile Inventories of the Terrestrial Planets (Abstract #2548). 52nd Lunar and Planetary Science Conference. CD-ROM.

Grossman, J. N. 2004. Loss of Chromium from Olivine During the Metamorphism of Chondrites (Abstract #1320). 35th Lunar and Planetary Science Conference. CD-ROM.

Grossman, L., and Larimer, J. W. 1974. Early Chemical History of the Solar System. *Reviews of Geophysics* 12: 71–101.

Grossman, L., and Olsen, E. 1974. Origin of the High-Temperature Fraction of C2 Chondrites. *Geochimica et Cosmochimica Acta* 38: 173–87.

Hamilton, V. E., Simon, A. A., Christensen, P. R., Reuter, D. C., Clark, B. E., Barucci, M. A., Bowles, N. E., et al. 2019. Evidence for Widespread Hydrated Minerals on Asteroid (101955) Bennu. *Nature Astronomy* 3: 332–40.

Hanowski, N. P., and Brearley, A. J. 2001. Aqueous Alteration of Chondrules in the CM Carbonaceous Chondrite, Allan Hills 81002: Implications for Parent Body Alteration. *Geochimica et Cosmochimica Acta* 65: 495–518.

Hewins, R. H., Bourot-Denise, M., Zanda, B., Leroux, H., Barrat, J.-A., Humayun, M., Göpel, C., et al. 2014. The Paris Meteorite, the Least Altered CM Chondrite So Far. *Geochimica et Cosmochimica Acta* 124: 190–222.

Hunt, G. R. 1979. Near-Infrared (1.3–2.4) μm Spectra of Alteration Minerals—Potential for Use in Remote Sensing. *Geophysics* 44: 1974–86.

Hutchison, R. 2004. *Meteorites: A Petrologic Chemical and Isotopic Synthesis*. Cambridge, UK: Cambridge University Press. 506.

Isa, J., Rubin, A. E., and Wasson, J. T. 2014. R-Chondrite Bulk-Chemical Compositions and Diverse Oxides: Implications for Parent-Body Processes. *Geochimica et Cosmochimica Acta* 124: 131–51.

Jenniskens, P., Fries, M. D., Yin, Q.-Z., Zolensky, M., Krot, A. N., Sandford, S. A., Sears, D., et al. 2012. Radar-Enabled Recovery of the Sutter's Mill Meteorite, a Carbonaceous Chondrite Regolith Breccia. *Science* 338: 1583–7.

Jilly, C. E., Huss, G. R., Krot, A. N., Nagashima, K., Yin, Q. Z., and Sugiura, N. 2014. ^{53}Mn-^{53}Cr Dating of Aqueously Formed Carbonates in the CM2 Lithology of the Sutter's Mill Carbonaceous Chondrite. *Meteoritics & Planetary Science* 49: 2104–17.

Jogo, K., Nagashima, K., Hutcheon, I. D., Krot, A. N., and Nakamura, T. 2013. Heavily Metamorphosed Clasts from the CV Chondrite Breccias Mokoia and Yamato-86009. *Meteoritics & Planetary Science* 47: 2251–68.

Joy, K. H., Tarte'se, R., Messenger, S., Zolensky, M. E., Marrocchi, Y., Frank, D. R., and Kring, D. A. 2020. The Isotopic Composition of Volatiles in the Unique Bench Crater Carbonaceous Chondrite Impactor Found in the Apollo 12 Regolith. *Earth and Planetary Science Letters* 540: 116265.

Kaplan, H. H., Lauretta, D. S., Simon, A. A., Hamilton, V. E., DellaGiustina, D. N., Golish, D. R., Reuter, D. C., et al. 2020. Bright Carbonate Veins on Asteroid (101955) Bennu: Implications for Aqueous Alteration History. *Science* 370: eabc3557.

Kerraouch, I., Bischoff, A., Zolensky, M. E., Pack, A., Patzek, M., Hanna, R. D., Fries, M. D., et al. 2021. The Polymict Carbonaceous Breccia Aguas Zarcas: A Potential Analog to Samples Being Returned by the OSIRIS-REx and Hayabusa2 Missions. *Meteoritics & Planetary Science* 56: 277–310.

Kerraouch, I., Ebert, S., Patzek, M., Bischoff, A., Zolensky, M. E., Pack, A., Schmitt-Kopplin, P., Belhai, D., Bendaoud, A., and Le, L. 2019. A Light, Chondritic Xenolith in the Murchison (CM) Chondrite–Formation by Fluid-Assisted Percolation During Metasomatism? *Geochemistry* 79: 125518.

Kerraouch, I., Kebukawa, Y., Bischoff, A., Zolensky, M. E., Wölfer, E., Hellmann, J. L., Ito, M., et al. 2022. Heterogeneous Nature of the Carbonaceous Chondrite breccia Aguas Zarcas–Cosmochemical Characterization and Origin of New Carbonaceous Chondrite Lithologies. *Geochimica et Cosmochimica Acta* 334: 155–86.

Kimura, M., Imae, N., Komatsu, M., Barrat, J. A., Greenwood, R. C., Yamaguchi, A., and Noguchi, T. 2020. The Most Primitive CM Chondrites, Asuka 12085, 12169, and 12236, of Subtypes 3.0–2.8: Their Characteristic Features and Classification. *Polar Science* 26: 100565.

King, A. J., Bates, H. C., Krietsch, D., Busemann, H., Clay, P. L., Schofield, P. F., and Russell, S. S. 2019. The Yamato-Type (CY) Carbonaceous Chondrite Group: Analogues for the Surface of Asteroid Ryugu? *Geochemistry* 79: 125531.

King, A. J., Russell, S. S., Schofield, P. F., Humphreys-Williams, E. R., Strekopytov, S., Abernethy, F. A. J., Verchovsky, A. B., and Grady, M. M. 2019. The Alteration History of the Jbilet Winselwan CM Carbonaceous Chondrite: An Analog for C-type Asteroid Sample Return. *Meteoritics & Planetary Science* 54: 521–43.

King, A. J., Schofield, P. F., and Russell, S. S. 2017. Type 1 Aqueous Alteration in CM Carbonaceous Chondrites: Implications for the Evolution of Water-Rich Asteroids. *Meteoritics & Planetary Science* 52: 1197–215.

King, A. J., Schofield, P. F., and Russell, S. S. 2020. CM Chondrites from Multiple Parent Bodies: Evidence from Correlated Mineralogy and Cosmic-Ray Exposure Ages (Abstract #1883). 51st Lunar and Planetary Science Conference. CD-ROM.

Kiseeva, E. S., and Wood, B. J. 2015. The Effects of Composition and Temperature on Chalcophile and Lithophile Element Partitioning into Magmatic Sulphides. *Earth and Planetary Science Letters* 424: 280–94.

Kitazato, K., Milliken, R. E., Iwata, T., Abe, M., Ohtake, M., Matsuura, S., Arai, T., et al. 2019. The Surface Composition of Asteroid 162173 Ryugu from Hayabusa2 Near-Infrared Spectroscopy. *Science* 364: 272–5. https://doi.org/10.1126/science.aav7432.

Krot, A. N., Keil K., Goodrich C. A., Scott E. R. D., and Weisberg M. K. 2003. Classification of Meteorites. In: *Meteorites, Comets, and Planets*, edited by H. D. Holland and K. K. Turekian. Treatise in Geochemistry, vol. 1, 83–128. Oxford: Elsevier-Pergamon.

Langbroek, M., Jenniskens, P., Kriegsman, L. M., Nieuwenhuis, H., De Kort, N. D., Kuiper, J., Van Westrenen, W., et al. 2019. The CM Carbonaceous Chondrite Regolith Diepenveen. *Meteoritics & Planetary Science* 54: 1431–61.

Lantz, C., Binzel, R. P., and DeMeo, F. E. 2018. Space Weathering Trends on Carbonaceous Asteroids: A Possible Explanation for Bennu's Blue Slope? *Icarus* 302: 10–7.

Lauretta, D. S., Bartels, A. E., Barucci, M. A., Bierhaus, E. B., Binzel, R. P., Bottke, W. F., Campins, H., et al. 2014. The OSIRIS-REx Target Asteroid (101955) Bennu: Constraints on its Physical, Geological, and Dynamical Nature from Astronomical Observations. *Meteoritics & Planetary Science* 50: 834–49. https://doi.org/10.1111/maps.12353.

Lebofsky, L. A. 1980. Infrared Reflectance Spectra of Asteroids: A Search for Water of Hydration. *The Astronomical Journal* 85: 573–85.

Lee, M. R., Cohen, B. E., King, A. J., and Greenwood, R. C. 2019. The Diversity of CM Carbonaceous Chondrite Parent Bodies Explored Using Lewis Cliff 85311. *Geochimica et Cosmochimica Acta* 264: 224–44.

Lee, M. R., and Ellen, R. 2008. Aragonite in the Murray (CM2) Carbonaceous Chondrite: Implications for Parent Body Compaction and Aqueous Alteration. *Meteoritics & Planetary Science* 43: 1219–31.

Lee, M. R., Lindgren, P., King, A. J., Greenwood, R. C., Franchi, I. A., and Sparkes, R. 2016. Elephant Moraine 96029, A Very Mildly Aqueously Altered and Heated CM Carbonaceous Chondrite: Implications for the Drivers of Parent Body Processing. *Geochimica et Cosmochimica Acta* 187: 237–59.

Lentfort, S., Bischoff, A., Ebert, S., and Patzek, M. 2021. Classification of CM Chondrite Breccias—Implications for the Evaluation of Samples from the OSIRIS-REx and Hayabusa 2 Missions. *Meteoritics & Planetary Science* 56: 127–47.

Li, S. J., Wang, S. J., Li, X. Y., Li, Y., Liu, S., and Coulson, I. M. 2012. A New Method for the Measurement of Meteorite Bulk Volume Via Ideal Gas Pycnometry. *Journal of Geophysical Research: Planets* 117: E10001.

Li, S. J., Wang, S. J., Miao, B. K., Li, Y., Li, X. Y., Zeng, X. J., and Xia, Z. P. 2019. The Density, Porosity, and Pore Morphology of Fall and Find Ordinary Chondrites. *Journal of Geophysical Research: Planets* 124: 2945–69.

Li, S. J., Yin, Q. Z., Bao, H., Sanborn, M. E., Irving, A., Ziegler, K., Agee, C., et al. 2018. Evidence for a Multilayered Internal Structure of the Chondritic Acapulcoite-Lodranite Parent Asteroid. *Geochimica et Cosmochimica Acta* 242: 82–101.

Lindgren, P., Hanna, R. D., Dobson, K. J., Tomkinson, T., and Lee, M. R. 2015. The Paradox Between Low Shock-Stage and Evidence for Compaction in CM Carbonaceous Chondrites Explained by Multiple Low-Intensity Impacts. *Geochimica et Cosmochimica Acta* 148: 159–78.

Lodders, K. 2003. Solar System Abundances and Condensation Temperatures of the Elements. *Astrophysical Journal* 591: 1220–47.

Lodders, K., and Fegley, B. 1998. *The Planetary Scientist's Companion*. New York: Oxford University Press on Demand.

Marrocchi, Y., Gounelle, M., Blanchard, I., Caste, F., and Kearsley, A. T. 2014. The Paris CM Chondrite: Secondary Minerals and Asteroidal Processing. *Meteoritics & Planetary Science* 49: 1232–49.

McSween, H. Y. 1979a. Are Carbonaceous Chondrites Primitive or Processed? *Reviews of Geophysics and Space Physics* 17: 1059–78.

McSween, H. Y. 1979b. Alteration in CM Carbonaceous Chondrites Inferred from Modal and Chemical Variations in Matrix. *Geochimica et Cosmochimica Acta* 43: 1761–70.

Metzler, K., Bischoff, A., and Stoffler, D. 1992. Accretionary Dust Mantles in Cm Chondrites – Evidence for Solar Nebula Processes. *Geochimica et Cosmochimica Acta* 56: 2873–97.

Michel, P., Ballouz, R. L., Barnouin, O. S., Jutzi, M., Walsh, K. J., May, B. H., Manzoni, C., et al. 2020. Collisional Formation of Top-Shaped Asteroids and Implications for the Origins of Ryugu and Bennu. *Nature Communications* 11: 1–11.

Miyamoto, M. 1991. Thermal Metamorphism of CI and CM Carbonaceous Chondrites: An Internal Heating Model. *Meteoritics* 26: 111–5.

Moriarty, G. M., Rumble, D., and Friedrich, J. M. 2009. Compositions of Four Unusual CM or CM-Related Antarctic Chondrites. *Geochemistry* 69: 161–8. https://doi.org/10.1016/j.chemer.2008.12.002.

Nakamura, T. 2006. Yamato 793321 CM Chondrite: Dehydrated Regolith Material of a Hydrous Asteroid. *Earth and Planetary Science Letters* 242: 26–38.

Nishiizumi, K., and Caffee, M. W. 2009. Exposure Histories of CM2 Carbonaceous Chondrites–An Update. *Meteoritics & Planetary Science Supplement* 72: 5358.

Nishiizumi, K., and Caffee, M. W. 2012. Exposure Histories of CI1 and CM1 Carbonaceous Chondrites (Abstract #2758). 43rd Lunar and Planetary Science Conference. CD-ROM.

Nishiizumi, K., Caffee, M. W., Hamajima, Y., Reedy, R. C., and Welten, K. C. 2014. Exposure History of the Sutter's Mill Carbonaceous Chondrite. *Meteoritics & Planetary Science* 49: 2056–63.

Patzek, M., Bischoff, A., Visser, R., and John, T. 2018. Mineralogy of Volatile-Rich Clasts in Brecciated Meteorites. *Meteoritics & Planetary Science* 53: 2519–40.

Piani, L., Marrocchi, Y., Rigaudier, T., Vacher, L. G., Thomassin, D., and Marty, B. 2020. Earth's Water May Have Been Inherited from Material Similar to Enstatite Chondrite Meteorites. *Science* 369: 1110–3.

Potin, S., Beck, P., Bonal, L., Schmitt, B., Garenne, A., Moynier, F., Agranier, A., Schmitt-Kopplin, P., Malik, A. K., and Quirico, E. 2020. Mineralogy, Chemistry, and Composition of Organic Compounds in the Fresh Carbonaceous Chondrite Mukundpura: CM1 or CM2? *Meteoritics & Planetary Science* 55: 1681–96.

Ray, D., and Shukla, A. D. 2018. The Mukundpura Meteorite, a New Fall of CM Chondrite. *Planetary and Space Science* 151: 149–54.

Rubin, A. E. 2010. Physical Properties of Chondrules in Different Chondrite Groups: Implications for Multiple Melting Events in Dusty Environments. *Geochimica et Cosmochimica Acta* 74: 4807–28.

Rubin, A. E., Trigo-Rodríguez, J. M., Huber, H., and Wasson, J. T. 2007. Progressive Aqueous Alteration of CM Carbonaceous Chondrites. *Geochimica et Cosmochimica Acta* 71: 2361–82.

Rudraswami, N. G., Naik, A. K., Tripathi, R. P., Bhandari, N., Karapurkar, S. G., Prasad, M. S., Babu, E. V. S. S. K., and Vijaya Sarathi, U. V. R. 2019. Chemical, Isotopic and Amino Acid Composition of Mukundpura CM2.0 (CM1) Chondrite: Evidence of Parent Body Aqueous Alteration. *Geoscience Frontiers* 10: 495–504.

Sanborn, M. E., Yamakawa, A., Yin, Q. Z., Irving, A. J., and Amelin, Y. 2013. Chromium Isotopic Studies of

Ungrouped Achondrites NWA 7325, NWA 2976, and NWA 6704. *Meteoritics & Planetary Science Supplement* 76: 5220.

Sanborn, M. E., and Yin, Q. Z. 2014. Chromium Isotopic Composition of the Anomalous Eucrites: An Additional Geochemical Parameter for Evaluating Their Origin (Abstract #A2018). 45th Lunar and Planetary Science Conference. CD-ROM.

Sanborn, M. E., Yin, Q. Z., and Irving, A. J. 2014. Isotope Forensics Utilizing $\Delta^{17}O$-^{54}Cr Systematics Provide Supporting Evidence for Differentiated Parent Bodies Overlain by Chondritic Veneers: A Case for the CR Parent Body (Abstract #2032). 45th Lunar and Planetary Science Conference. CD-ROM.

Sanborn M. E., Yin Q. Z., Rumble D., Kuehner S. M., and Irving A. J. 2014. Re-Evaluation of Anomalous Metal-Rich Lodranite Northwest Africa 468 Based on Combined Chromium and Oxygen Isotopes (Abstract). Annual Meeting of the Meteoritical Society 77, 5169.

Schmitz, B., Yin, Q. Z., Sanborn, M. E., Tassinari, M., Caplan, C. E., and Huss, G. R. 2016. A New Type of Solar-System Material Recovered from Ordovician Marine Limestone. *Nature Communications* 7: 11851.

Scott E. R. D., and Krot A. N. 2014. Chondrites and Their Components. In *Treatise on Geochemistry*. *Meteorites and Cosmochemical Processes*, vol. 1, revised edition. Oxford: Elsevier. pp. 65–137.

Sharp, Z. D. 1990. A Laser-Based Microanalytical Method for the In Situ Determination of Oxygen Isotope Ratios of Silicates and Oxides. *Geochimica et Cosmochimica Acta* 54: 1353–7.

Simon, A. A., Kaplan, H. H., Hamilton, V. E., Lauretta, D. S., Campins, H., Emery, J. P., Barucci, M. A., et al. 2020. Widespread Carbon-Bearing Materials on Near-Earth Asteroid (101955) Bennu. *Science* 370: eabc3522.

Sugita, S., Honda, R., Morota, T., Kameda, S., Sawada, H., Tatsumi, E., Yamada, M., et al. 2019. The Geomorphology, Color, and Thermal Properties of Ryugu: Implications for Parent-Body Processes. *Science* 364: 252.

Sunshine, J. M., Farnham, T. L., Feaga, L. M., Groussin, O., Merlin, F., Milliken, R. E., and A'Hearn, M. F. 2009. Temporal and Spatial Variability of Lunar Hydration as Observed by the Deep Impact Spacecraft. *Science* 326: 565–8.

Suttle, M. D., King, A. J., Schofield, P. F., Bates, H., and Russell, S. S. 2021. The Aqueous Alteration of CM Chondrites, A Review. *Geochimica et Cosmochimica Acta* 299: 219–56.

Takir, D., Emery, J. P., Mcsween, H. Y., Jr., Hibbitts, C. A., Clark, R. N., Pearson, N., and Wang, A. 2013. Nature and Degree of Aqueous Alteration in CM and CI Carbonaceous Chondrites. *Meteoritics & Planetary Science* 48: 1618–37.

Tatsumi, E., Popescu, M., Campins, H., De León, J., García, J. L. R., Licandro, J., Simon, A. A., et al. 2021. Widely Distributed Exogenic Materials of Varying Compositions and Morphologies on Asteroid (101955) Bennu. *Monthly Notices of the Royal Astronomical Society* 508: 2053–70.

Thompson, M. S., Loeffler, M. J., Morris, R. V., Keller, L. P., and Christoffersen, R. 2019. Spectral and Chemical Effects of Simulated Space Weathering of the Murchison CM2 Carbonaceous Chondrite. *Icarus* 319: 499–511.

Tomeoka, K., and Buseck, P. R. 1985. Indicators of Aqueous Alteration in CM Carbonaceous Chondrites: Microtextures of a Layered Mineral Containing Fe, S, O and Ni. *Geochimica et Cosmochimica Acta* 49: 2149–63.

Tonui, E., Zolensky, M., Hiroi, T., Nakamura, T., Lipschutz, M. E., Wang, M.-S., and Okudaira, K. 2014. Petrographic, Chemical and Spectroscopic Evidence for Thermal Metamorphism in Carbonaceous Chondrites I: CI and CM Chondrites. *Geochimica et Cosmochimica Acta* 126: 284–306.

Torrano, Z. A., Schrader, D. L., Davidson, J., Greenwood, R. C., Dunlap, D. R., and Wadhwa, M. 2021. The Relationship Between CM and CO Chondrites: Insights from Combined Analyses of Titanium, Chromium, and Oxygen Isotopes in CM, CO, and Ungrouped Chondrites. *Geochimica et Cosmochimica Acta* 301: 70–90.

Velbel, M. A., Tonui, E. K., and Zolensky, M. E. 2012. Replacement of Olivine by Serpentine in the Carbonaceous Chondrite Nogoya (CM2). *Geochimica et Cosmochimica Acta* 87: 117–35.

Velbel, M. A., Tonui, E. K., and Zolensky, M. E. 2015. Replacement of Olivine by Serpentine in the Queen Alexandra Range 93005 Carbonaceous Chondrite (CM2): Reactant–Product Compositional Relations, and Isovolumetric Constraints on Reaction Stoichiometry and Elemental Mobility During Aqueous Alteration. *Geochimica et Cosmochimica Acta* 148: 402–25.

Velbel, M. A., and Zolensky, M. E. 2021. Thermal Metamorphism of CM Chondrites: A Dehydroxylation-Based Peak-Temperature Thermometer and Implications for Sample Return from Asteroids Ryugu and Bennu. *Meteoritics & Planetary Science* 56: 546–85.

Verdier-Paoletti, M. J., Marrocchi, Y., Avice, G., Roskosz, M., Gurenko, A., and Gounelle, M. 2016. Oxygen Isotope Constraints on the Alteration Temperatures of CM Chondrites. *Earth & Planetary Science Letters* 458: 273–81.

Vilas, F. 2008. Spectral Characteristics of Hayabusa 2 Near-Earth Asteroid Targets 162173 1999 JU3 and 2001 QC34. *The Astronomical Journal* 135: 1101–5.

Warren, P. H. 2011a. Stable-Isotopic Anomalies and the Accretionary Assemblage of the Earth and Mars: a Subordinate Role for Carbonaceous Chondrites. *Earth & Planetary Science Letters* 311: 93–100.

Warren, P. H. 2011b. Stable Isotopes and the Noncarbonaceous Derivation of Ureilites, in Common with Nearly all Differentiated Planetary Materials. *Geochimica et Cosmochimica Acta* 75: 6912–26.

Wasson, J. T., and Kallemeyn, G. W. 1988. Compositions of Chondrites. *Philosophical Transactions of the Royal Society of London Series A, Mathematical and Physical Sciences* 325: 535–44.

Weisberg, M. K., McCoy, T. J., and Krot, A. N. 2006. Systematics and Evaluation of Meteorite Classification. In *Meteorites and the Early Solar System II*, edited by D. S. Lauretta and H. Y. McSween, Jr., 19–52. Tucson, Arizona: University of Arizona Press.

Wiik, H. B. 1956. The Chemical Composition of Some Stony Meteorites. *Geochimica et Cosmochimica Acta* 9: 279–89.

Wlotzka, F. 2005. Cr Spinel and Chromite as Petrogenetic Indicators in Ordinary Chondrites: Equilibration Temperatures of Petrologic Types 3.7 to 6. *Meteoritics & Planetary Science* 40: 1673–702.

Wlotzka, F., Spettel, B., Palme, H., and Schultz, L. 1989. Two new CM Chondrites from Antarctica: Different Mineralogy, but Same Chemistry. *Meteoritics* 24: 341.

Wu, J., Desch, S. J., Schaefer, L., Elkins-Tanton, L. T., Pahlevan, K., and Buseck, P. R. 2018. Origin of Earth's

Water: Chondritic Inheritance Plus Nebular Ingassing and Storage of Hydrogen in the Core. *Journal of Geophysical Research: Planets* 123: 2691–712.

Yamakawa, A., Yamashita, K., Makishima, A., and Nakamura, E. 2009. Chemical Separation and Mass Spectrometry of Cr, Fe, Ni, Zn, and Cu in Terrestrial and Extraterrestrial Materials Using Thermal Ionization Mass Spectrometry. *Analytical Chemistry* 81: 9787–94.

Yamakawa, A., and Yin, Q. Z. 2014. Chromium Isotopic Systematics of the Sutter's Mill Carbonaceous Chondrite: Implications for Isotopic Heterogeneities of the Early Solar System. *Meteoritics & Planetary Science* 49: 2118–27.

Yin, Q. Z., Yamashita, K., Yamakawa, A., Tanaka, R., Jacobsen, B., Ebel, D., Hutcheon, I. D., and Nakamura, E. 2009. ^{53}Mn-^{53}Cr Systematics of Allende Chondrules and ε^{54}Cr—Δ^{17}O Correlation in Bulk Carbonaceous Chondrites (Abstract #A2006). 40th Lunar and Planetary Science Conference. CD-ROM.

Yokoyama, T., Nagashima, K., Nakai, I., Young, E. D., Abe, Y., Aléon, J., Alexander, C. M. O'D., et al. 2022. Samples Returned from the Asteroid Ryugu Are Similar to Ivuna-Type Carbonaceous Meteorites. *Science*. https://doi.org/10.1126/science.abn7850.

Zega, T. 2004. Serpentine Nanotubes in the Mighei CM Chondrite. *Earth and Planetary Science Letters* 223: 141–6.

Zhang, A., Guan, Y., Hsu, W., Liu, Y., and Taylor, L. A. 2010. Origin of a Metamorphosed Lithic Clast in CM Chondrite Grove Mountains 021536. *Meteoritics & Planetary Science* 45: 238–45.

Zhang, P. F., Tai, K. R., Li, Y., Zhang, J., Lantz, C., Hiroi, T., Matsuoka, M., et al. 2022. Diverse Space Weathering Effects on Asteroid Surfaces as Inferred via Laser Irradiation of Meteorites. *Astronomy & Astrophysics* 659: A78.

Zhang, P. F., Zhang, J., Li, S. J., Liu, C. Q., Wen, Y. Y., Sun, H., and Li, Y. 2020. Laboratory Simulation of the Space Weathering Effects on Reflectance Spectra of Near-Earth Asteroids. *Bulletin of Mineralogy, Petrology and Geochemistry* 39: 179–87. In Chinese with English abstract.

Zhu, K., Moynier, F., Schiller, M., Becker, H., Barrat, J. A., and Bizzarro, M. 2021. Tracing the Origin and Core Formation of the Enstatite Achondrite Parent Bodies Using Cr Isotopes. *Geochimica et Cosmochimica Acta* 308: 256–72.

Zolensky, M., Barrett, R., and Browning, L. 1993. Mineralogy and Composition of Matrix and Chondrule Rims in Carbonaceous Chondrites. *Geochimica et Cosmochimica Acta* 57: 3123–48. https://doi.org/10.1016/0016-7037(93)90298-b.

Zolensky, M. E., Hewins, R. H., Mittlefehldt, D. W., Lindstrom, M. M., Xiao, X., and Lipschutz, M. E. 1992. Mineralogy, Petrology and Geochemistry of Carbonaceous Chondritic Clasts in the LEW 85300 Polymict Eucrite. *Meteoritics* 27: 596–604.

Zolensky, M., and Ivanov, A. 2003. The Kaidun Microbreccia Meteorite: A Harvest from the Inner and Outer Asteroid Belt. *Geochemistry* 63: 185–246.

Zolensky, M., and McSween, H. Y. 1988. Aqueous Alteration. In *Meteorites and the Early Solar System*, edited by J. F. Kerridge and M. S. Matthews, 114–43. Tucson, Arizona: University of Arizona Press.

Zolensky, M., Mikouchi, T., Fries, M., Bodnar, R., Jenniskens, P., Yin, Q. Z., Hagiya, K., et al. 2014. Mineralogy and Petrography of C Asteroid Regolith: The Sutter's Mill CM Meteorite. *Meteoritics & Planetary Science* 49: 1997–2016.

Zolensky, M. E., Mittlefehldt, D. W., Lipschutz, M. E., Wang, M. S., Clayton, R. N., Mayeda, T. K., Grady, M. M., Pillinger, C., and Barber, D. 1997. CM Chondrites Exhibit the Complete Petrologic Range from Type 2 to 1. *Geochimica et Cosmochimica Acta* 61: 5099–115.

Zolensky, M. E., Takenouchi, A., Mikouchi, T., Gregory, T., Nishiizumi, K., Caffee, M. W., Velbel, M. A., et al. 2020. The Nature of the CM Parent Asteroid Regolith Based on Cosmic Ray Exposure Ages. *Meteoritics & Planetary Science* 56: 49–55.

Zolensky, M. E., Weisberg, M. K., Buchanan, P. C., and Mittlefehldt, D. W. 1996. Mineralogy of Carbonaceous Chondrite Clasts in HED Achondrites and the Moon. *Meteoritics & Planetary Science* 31: 518–37.